Article

Cell

Engineered Sialylation of Pathogenic Antibodies *In Vivo* Attenuates Autoimmune Disease

Graphical Abstract

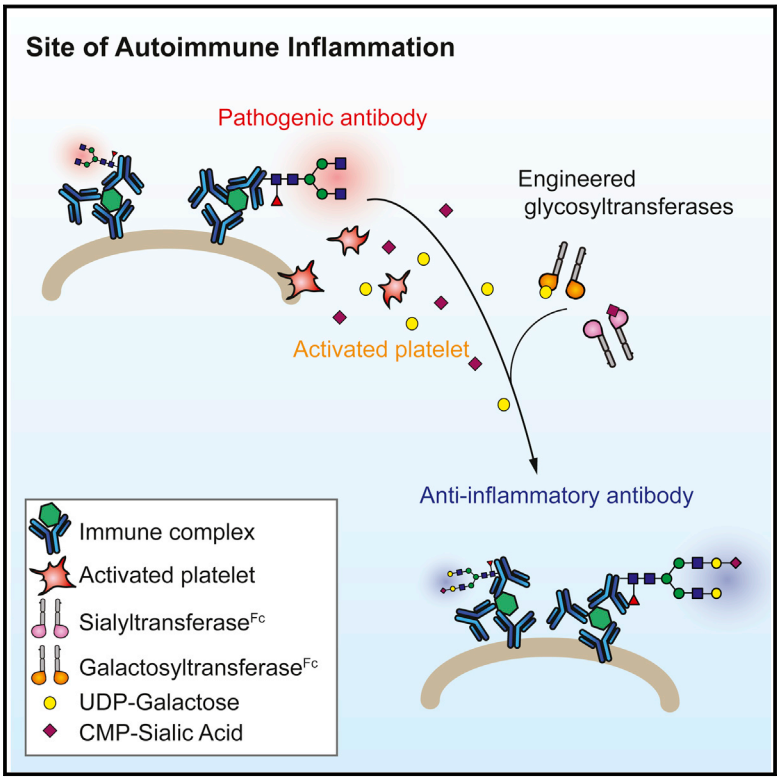

Highlights

- Glycosyltransferase fusions convert endogenous IgG into anti-inflammatory IgG
- Platelets enable site-specific sialylation by releasing sugar-nucleotide donors
- Inhibitory FcγRIIB, STAT6, and type II FcγRs are required for anti-inflammatory activity

Authors

Jose D. Pagan, Maya Kitaoka, Robert M. Anthony

Correspondence

robert.anthony@mgh.harvard.edu

In Brief

Endogenous pathogenic antibodies can be enzymatically converted into anti-inflammatory mediators in inflamed tissues, revealing a new strategy to treat autoimmune diseases.

Pagan et al., 2018, Cell *172*, 564–577
January 25, 2018
https://doi.org/10.1016/j.cell.2017.11.041

CellPress

Engineered Sialylation of Pathogenic Antibodies *In Vivo* Attenuates Autoimmune Disease

Jose D. Pagan,[1,2] Maya Kitaoka,[1,2] and Robert M. Anthony[1,3,*]
[1]Center for Immunology and Inflammatory Diseases, Division of Rheumatology, Allergy, and Immunology, Department of Medicine, Massachusetts General Hospital and Harvard Medical School, Boston, MA 02129, USA
[2]These authors contributed equally
[3]Lead Contact
*Correspondence: robert.anthony@mgh.harvard.edu
https://doi.org/10.1016/j.cell.2017.11.041

SUMMARY

Self-reactive IgGs contribute to the pathology of autoimmune diseases, including systemic lupus erythematosus and rheumatoid arthritis. Paradoxically, IgGs are used to treat inflammatory diseases in the form of high-dose intravenous immunoglobulin (IVIG). Distinct glycoforms on the IgG crystallizable fragment (Fc) dictate these divergent functions. IgG anti-inflammatory activity is attributed to sialylation of the Fc glycan. We therefore sought to convert endogenous IgG to anti-inflammatory mediators *in vivo* by engineering solubilized glycosyltransferases that attach galactose or sialic acid. When both enzymes were administered in a prophylactic or therapeutic fashion, autoimmune inflammation was markedly attenuated *in vivo*. The enzymes worked through a similar pathway to IVIG, requiring DC-SIGN, STAT6 signaling, and FcγRIIB. Importantly, sialylation was highly specific to pathogenic IgG at the site of inflammation, driven by local platelet release of nucleotide-sugar donors. These results underscore the therapeutic potential of glycoengineering *in vivo*.

INTRODUCTION

Immunoglobulin gamma (IgG) antibodies are the preeminent effector proteins of the immune system. They are essential for clearance of microbes by bridging the adaptive and innate immune systems, but they can also contribute to the pathogenesis of autoimmune diseases when they are generated against self (Nimmerjahn and Ravetch, 2008b). The bimodal activity of IgG antibodies allows simultaneous recognition of antigen by the antigen-binding fragment (Fab, Figure 1A) with high affinity and recruitment and activation of leukocytes through interactions between the crystallizable fragment (Fc, Figure 1A) and Fc gamma receptors (FcγRs) on innate immune cells (Nimmerjahn et al., 2015). This triggers the canonical inflammatory effector functions of IgG, including antibody-dependent cytotoxicity (ADCC) and uptake of recognized antigens (Franklin, 1975; Huber et al., 1976).

A single N-linked glycan is present on each heavy chain of all IgG and positioned at asparagine-297 in the Fc (N-297, Figures 1A and 1B) (Arnold et al., 2007). The core heptasaccharide of the glycan has a complex biantennary structure that can vary by the addition of fucose, *N*-acetylglucosamine (GlcNAc), galactose, or sialic acid (Figure 1B). These variable additions account for tremendous heterogeneity, with over 30 distinct glycans identified on circulating IgG in healthy individuals (Kaneko et al., 2006b). Studies over the last decade have demonstrated the composition of the Fc glycan exerts profound influence over IgG effector functions (Jefferis, 2005, 2009a, 2009b). IgG with afucosylated Fc glycans have 50-fold enhanced affinity to the activating FcγR, FcγRIIIA, compared to fucosylated IgG and exhibit markedly enhanced ADCC *in vivo* (Ferrara et al., 2011; Natsume et al., 2005; Okazaki et al., 2004; Shields et al., 2002). Recent studies have linked dengue-specific IgG with afucosylated Fc glycans with Dengue hemorrhagic fever (Wang et al., 2017) and tuberculosis (TB)-specific afucosylated IgG in controlling latent TB infections (Lu et al., 2016). The most successful HIV vaccine trial to date resulted in increased levels of bisecting GlcNAc on IgG Fc glycans, a modification that also increases affinity to FcγRIIIA, albeit to a lesser extent than afucosylation (Ackerman et al., 2013; Chung et al., 2014; Davies et al., 2001). Conversely, terminal sialylation of the Fc glycan reduces IgG affinity for type I FcγRs, and sialylated IgG have reduced capacity to initiate ADCC *in vivo* (Anthony et al., 2008a; Li et al., 2017; Scallon et al., 2007). Enhanced IgG sialylation following influenza vaccination was attributed to improved affinity maturation through a type II FcγR-CD23 pathway (Wang et al., 2015). Although the regulation of IgG glycosylation is not completely understood, IL-23 has been implicated in regulating sialyltransferase ST6GAL1 expression (Pfeifle et al., 2017).

Paradoxically, IgG is commonly used in the clinic to suppress inflammation (Negi et al., 2007). Intravenous immunoglobulin (IVIG) is a therapeutic preparation of polyclonal IgG derived from thousands of healthy donors and has successfully been used in the clinic for almost 40 years at a high dose (1–2 g/kg) for the treatment of inflammatory and autoimmune diseases (Imbach et al., 1981; Nimmerjahn and Ravetch, 2008a). Mechanistic studies revealed that the Fc portion of IVIG was sufficient for anti-inflammatory activity *in vivo* (Debré et al., 1993; Samuelsson et al., 2001), requiring the inhibitory FcγRIIB (Samuelsson et al., 2001; Schwab et al., 2012; Schwab et al.,

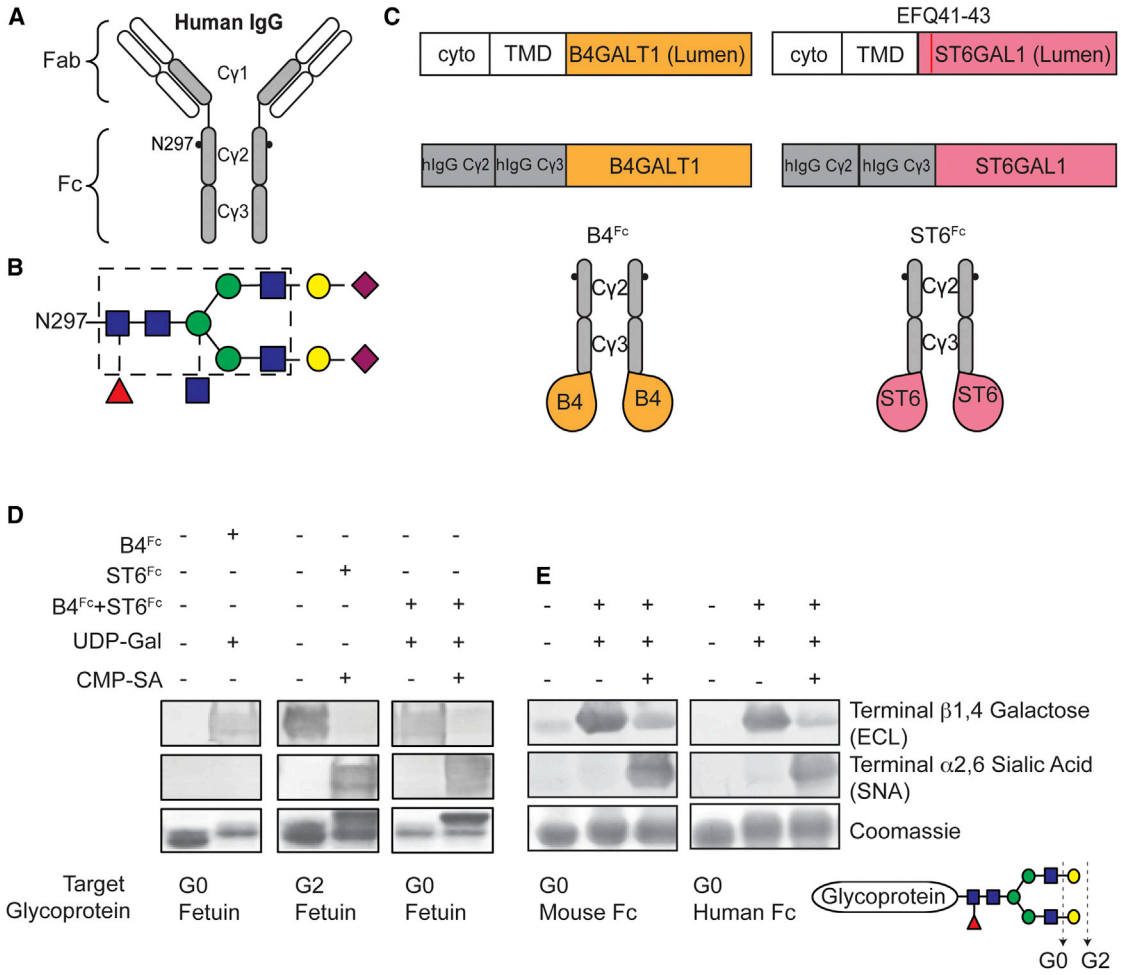

Figure 1. Solubilizing and Engineering Glycosyltransferase Enzymes

(A) IgG Fab and Fc with a single, N-linked glycosylation site at N297.

(B) Fc glycan core shown in the box consists of GlcNAc (blue squares) and mannose (green circles); variable additions include fucose (red triangle), bisecting GlcNAc, galactose (yellow circles), or sialic acid (purple diamonds).

(C) *trans*-Golgi enzymes B4GALT1 and ST6GAL1 have cytoplasmic (cyto), transmembrane (TMD), and enzymatic luminal domains (Lumen). ST6GAL1 cleavage site EFQ41-43 is indicated by a red line.

(D and E) Lectin blots for terminal galactose (ECL) or sialic acid (SNA) on target glycoproteins fetuin (D) or mouse and human IgG Fcs (E).

See also Figure S1 and Table S1.

2014; Tackenberg et al., 2009; Tackenberg et al., 2010). Further, sialylation of the Fc glycan was essential for this activity (Anthony et al., 2008a; Kaneko et al., 2006b). Instead of binding the activating type I FcγRs, sialylated IgG Fc bound type II FcγRs, human dendritic cell-specific ICAM3-grabbing non-integrin (DC-SIGN), or murine SIGN-R1, culminating in increased surface expression of the inhibitory FcγRIIB on inflammatory effector cells (Anthony et al., 2011; Anthony et al., 2008b; Samuelsson et al., 2001). Indeed, alternative mechanisms through which high-dose IVIG suppresses inflammation, including Fab- or FcRn-dependent mechanisms, have been proposed (Hansen and Balthasar, 2002; Li et al., 2005; Schwab and Nimmerjahn, 2014). Further, the role of IgG sialylation in the immunomodulatory activity of IVIG has been challenged, likely due to technical difficulties generating of sialylated IgG Fcs or particulars of distinct experimental systems (Bayry et al., 2009; Campbell et al., 2014). Importantly, a number of groups have reported anti-inflammatory activity of IgG sialylation (Ohmi et al., 2016; Schwab et al., 2012; Washburn et al., 2015). Thus, sialylation of the Fc glycan, along with DC-SIGN and FcγRIIB, constitute a general anti-inflammatory pathway of IgG *in vivo* (Anthony et al., 2011; Kaneko et al., 2006b; Tackenberg et al., 2009; Washburn et al., 2015).

Glycans are attached and modified to proteins passing through the secretory pathway in the endoplasmic reticulum (ER) and Golgi. While B cells, plasma cells, and cytokine milieu are implicated in regulating IgG glycosylation, recent evidence suggests that glycans can be modified extracellularly (Jones et al., 2016; Ohmi et al., 2016; Pfeifle et al., 2017; Wang et al., 2015). A soluble form of the sialyltransferase ST6GAL1

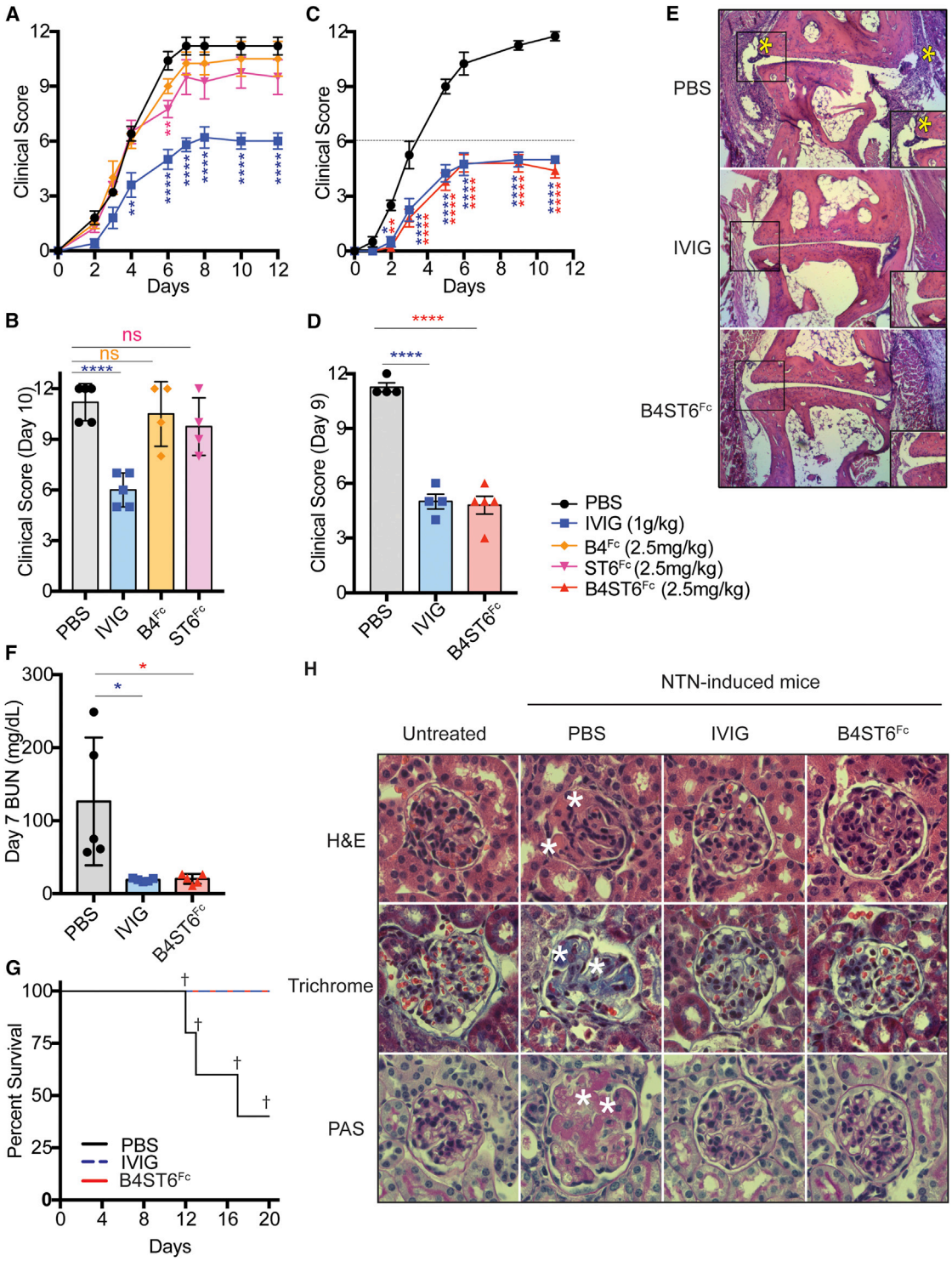

Figure 2. Anti-inflammatory Activity of *In Vivo* Sialylation

(A) Clinical scores of mice treated with K/BxN and PBS (black circles), ST6^{Fc} (pink triangles), B4^{Fc} (orange diamonds), or IVIG (blue squares).

(B) Day 10 scores from (A) are plotted.

(C) Clinical scores of K/BxN treated mice given PBS (black circles), IVIG (blue squares), or B4ST6^{Fc} (red triangles).

(D) Day 9 scores from (C) are shown.

(E) H&E of paw sections 7 days after K/BxN sera and PBS, IVIG, or B4ST6^{Fc}.

(F and G) Day 7 BUN levels (F) and survival (G) of mice induced with NTN and treated with PBS (black circles), IVIG (blue squares), or B4ST6^{Fc} (red triangles).

(legend continued on next page)

is released into the circulation by hepatocytes and is enzymatically active (Jones et al., 2012; Sugimoto et al., 2007). Selective disruption of hepatic ST6GAL1 expression (Kalcheva et al., 1997; Wang et al., 1993) reduced levels of IgG sialylation. Conversely, B cell-specific deletion of ST6GAL1 had little effect on IgG sialylation (Jones et al., 2016), suggesting that extracellular sialylation may occur during homeostasis. We therefore asked whether we could increase IgG sialylation *in vivo* by administering a soluble ST6GAL1 and thus convert inflammatory IgGs into anti-inflammatory mediators in autoimmune disease.

RESULTS

Engineering Soluble Glycosyltransferases

ST6GAL1 catalyzes attachment of α2,6 sialic acid to galactose on N-linked glycans (Meng et al., 2013). Sialylation canonically occurs in the *trans*-Golgi, where the ST6GAL1 is anchored by a transmembrane domain (TMD, Figure 1C). A β-secretase (BACE1) cleavage site is present in the luminal domain of ST6GAL1 at EFQ41-43, which results in ST6GAL1 secretion (Figures 1C and S1) (Woodard-Grice et al., 2008). The extraordinary effects of sialylation on IgG biology prompted us to explore the therapeutic potential of glycoengineering IgG *in vivo*.

To this end, we fused glycosylation enzymes to human IgG1 Fc—a common approach to generate soluble forms of membrane proteins. Expression constructs with fusions of Fc and ST6GAL1 that included the region upstream of EFQ41-43 in the amino acid sequence resulted in multiple protein products, consistent with BACE1 activity (Figure S1). However, when the Fc was linked directly to E41, omitting the first 40 amino acids of ST6GAL1, a single product was generated ($ST6^{Fc}$; Figures 1C, S1B, and S1C). We took a similar approach with the B4GALT1 enzyme responsible for attachment of galactose to the IgG Fc glycan, because sialylation efficiency improves with increased galactose content (Anthony et al., 2008a). The engineered fusions of B4GALT1 luminal domains with human IgG1 Fc resulted in a single protein product ($B4^{Fc}$, Figures 1C and S1C). The engineered glycosyltransferases were determined to be the correct molecular weight and recognized by antibodies specific for B4GALT1, ST6GAL1, and human IgG by immunoblotting (Figure S1D).

Next, we examined the activity of engineered enzymes *in vitro* using fetuin, a highly glycosylated protein, as a target for glycoengineering. Fetuin was treated with glycosidases to remove sialic acid and galactose residues, generating asialylated, galactosylated (G2), and agalactosylated (G0) fetuin (Figure 1D). We incubated G0 and G2 fetuin with $B4^{Fc}$, $ST6^{Fc}$, or with both enzymes ($B4ST6^{Fc}$) and sugar-nucleotide donors (uridine diphosphate [UDP]-galactose [UDP-Gal] and CMP-sialic acid [CMP-SA] for galactose and sialic acid, respectively). Linkage-specific glycosylation by lectin blotting revealed that $B4^{Fc}$ efficiently attached terminal galactose in β1,4 linkages and $ST6^{Fc}$ attached α2,6 terminal sialic acid (Figure 1D). $B4ST6^{Fc}$ added β1,4 galactose when incubated with a galactose donor (UDP-Gal, Figure 1D). $B4ST6^{Fc}$ efficiently sialylated fetuin when incubated with both galactose and sialic acid donors (Figure 1D). Further, $B4ST6^{Fc}$ transferred galactose and sialic acid to both mouse and human IgG (Figure 1E).

Anti-inflammatory Activity of *In Vivo* Sialylation

Next, we examined the ability of these engineered glycosylation enzymes to attenuate inflammation *in vivo*. Mice were given arthritogenic K/BxN sera, which initiates joint inflammation—mediated primarily by IgG1 autoantibodies—that presents with edema and inflammatory cell infiltration within days after treatment (Kouskoff et al., 1996). Animals also received PBS, high-dose IVIG (1 g/kg), $B4^{Fc}$ (2.5 mg/kg), $ST6^{Fc}$ (2.5 mg/kg), or both $B4^{Fc}$ and $ST6^{Fc}$ ($B4ST6^{Fc}$, 2.5 mg/kg, Figures 2A–2E). The arthritogenic sera induced robust inflammation in PBS-treated animals as measured by clinical score, while inflammation was attenuated by IVIG (Figures 2A and 2B). Neither $B4^{Fc}$ nor $ST6^{Fc}$ individually was able to reduce induced inflammation. However, when the engineered enzymes were co-administered ($B4ST6^{Fc}$, 2.5 mg/kg), inflammation was significantly reduced, mirroring IVIG (Figures 2C and 2D). The inflammatory cells infiltrating the joint and tissue destruction 7 days after treatment were markedly reduced in IVIG- and $B4ST6^{Fc}$-treated animals compared to PBS-treated controls (Figure 2E).

To extend these findings to an active model of autoimmune disease, we turned to a model of Goodpasture disease that results in nephrotoxic-nephritis (NTN)-driven predominantly kidney-deposited IgG2b-based immune complexes (Kaneko et al., 2006a; Lerner et al., 1967; Schrijver et al., 1990). Administration of $B4ST6^{Fc}$ suppressed kidney pathology as effectively as IVIG, as measured by blood urea nitrogen (BUN) levels at day 7 (Figure 2F) and survival (Figure 2G). Indeed, inflammatory cell infiltration into the kidneys at day 7 and glomerulosclerosis scoring was reduced by $B4ST6^{Fc}$ and IVIG compared to PBS controls (Figures 2H and S2A). Neither IVIG nor $B4ST6^{Fc}$ affected the induced pathogenic antibody response, as measured by serum or kidney IgG titers (Figures S2B and S2C). Together, these results demonstrate that administration of enzymes that attach both galactose and sialic acid are effective at attenuating autoimmune inflammation *in vivo* similarly to immunomodulatory high-dose IVIG.

Requirements for *In Vivo* Sialylation

The requirements of the inhibitory FcγRIIB for the anti-inflammatory activity of IVIG and sialylated IgG Fc were demonstrated by functional studies using murine models (Anthony et al., 2011; Bruhns et al., 2003; Samuelsson et al., 2001; Schwab et al., 2014) and supported by increased surface expression of FcγRIIB on leukocytes following administration of high-dose IVIG to chronic inflammatory demyelinating polyneuropathy

(H) H&E, trichrome, and periodic acid shift (PAS) staining of kidney sections from untreated or NTN-treated mice 7 days following PBS, IVIG, or $B4ST6^{Fc}$ administration.

Means and standard deviation are plotted. Results are representative of at least two independent repeats. *$p < 0.05$, **$p < 0.01$, ***$p < 0.005$, ****$p < 0.001$, not significant (ns), determined by two-way ANOVA followed by Tukey's test. See also Figure S2.

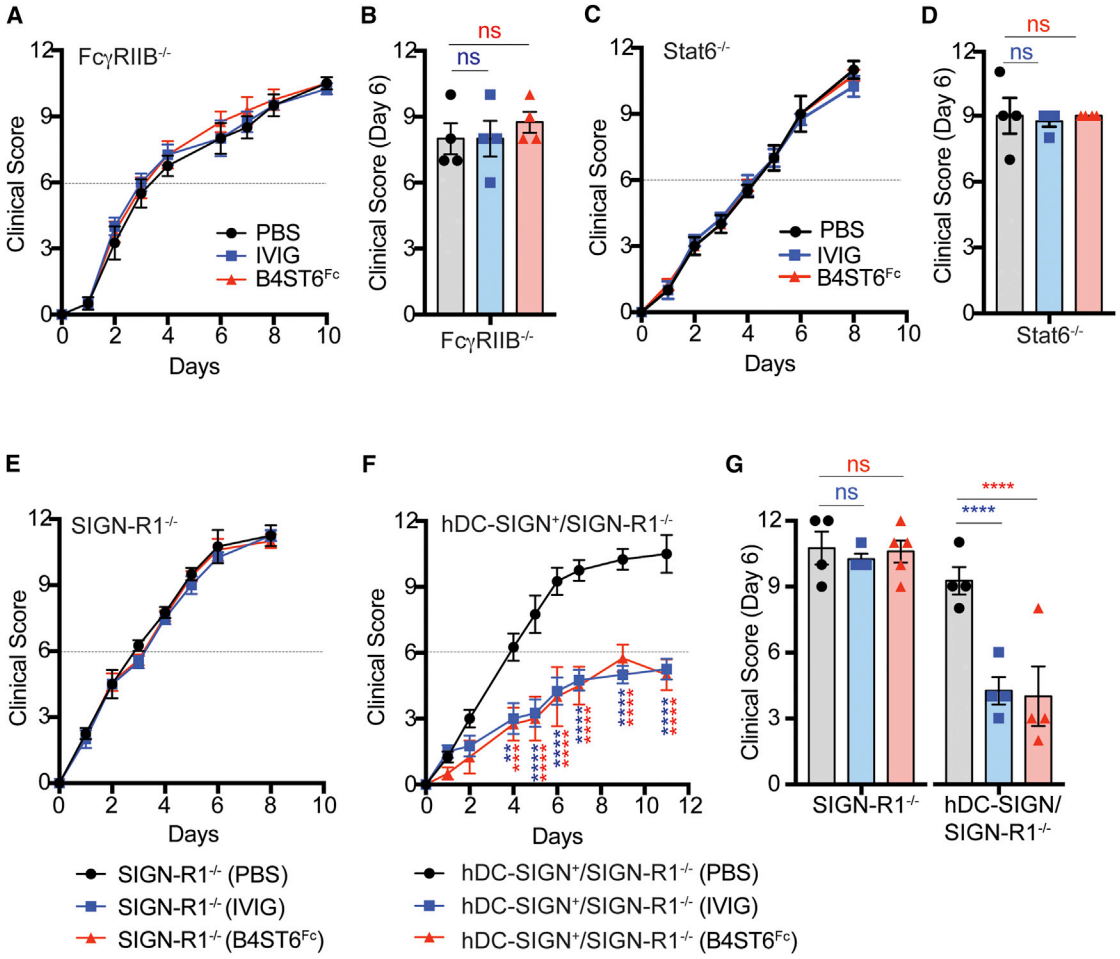

Figure 3. Receptor Requirements for *In Vivo* Sialylation

(A) Clinical scores of FcγRIIB$^{-/-}$ mice given K/BxN sera and PBS (black circles), IVIG (blue squares), or B4ST6^{Fc} (red triangles).

(B) Day 6 scores from (A) are plotted.

(C) Clinical scores of STAT6$^{-/-}$ mice given K/BxN sera and PBS (black circles), IVIG (blue squares), or B4ST6^{Fc} (red triangles).

(D) Day 6 scores from (C) are shown.

(E and F) Clinical scores of (E) SIGN-R1$^{-/-}$ and (F) hDC-SIGN^{+}/SIGN-R1$^{-/-}$ mice given K/BxN sera and PBS (black circles), IVIG (blue squares), or B4ST6^{Fc} (red triangles).

(G) Day 6 scores from (E) and (F) are shown.

Means and standard deviation are plotted. Results are representative of at least two independent repeats. **$p < 0.01$, ***$p < 0.005$, ****$p < 0.001$, ns, determined by two-way ANOVA followed by Tukey's test. See also Figures S3 and S4.

patients (Tackenberg et al., 2009). Sialylated IgG Fcs were shown to require murine SIGN-R1 or human DC-SIGN to suppress inflammation through a Th2 pathway involving IL-4 receptor signaling through STAT6 (Anthony et al., 2011; Anthony et al., 2008b; Schwab et al., 2012). Thus, sialylation of IgG converts receptor preference to type II FcγRs such that ligation of type II FcγRs by sialylated IgG initiates an anti-inflammatory cascade culminating in increased inhibitory FcγRIIB expression on inflammatory cells (Pincetic et al., 2014). We asked whether *in vivo* sialylation suppressed inflammation through a similar pathway and administered K/BxN sera along with PBS, IVIG, or B4ST6^{Fc} to FcγRIIB$^{-/-}$, STAT6$^{-/-}$, and wild-type (WT) mice. Neither IVIG nor B4ST6^{Fc} suppressed inflammation relative to PBS (Figures 3A, 3B, and S3A) in FcγRIIB$^{-/-}$ mice. Similarly, neither IVIG nor B4ST6^{Fc} suppressed K/BxN-induced inflammation (Figures 3C, 3D, and S3B) in STAT6$^{-/-}$ mice. Next, we administered K/BxN sera and PBS, IVIG, or B4ST6^{Fc} to SIGN-R1$^{-/-}$ and human DC-SIGN transgenic mice that were crossed to a SIGN-R1$^{-/-}$ background (hDC-SIGN^{+}/SIGN-R1$^{-/-}$, Figures 3E–3G). K/BxN sera transfer, along with PBS treatment, resulted in robust inflammation in both genotypes (Figures 3E and 3F). SIGN-R1$^{-/-}$ animals were not protected from induced arthritis by IVIG or B4ST6^{Fc} (Figure 3E). Consistently, administration of an antibody that results in transient knockdown of SIGN-R1 revealed no differences in mice following treatment with K/BxN and PBS, IVIG, or B4ST6^{Fc} (TKO SIGN-R1, Figures S3C and S3D) (Kang et al., 2004). However, both IVIG and B4ST6^{Fc} attenuated induced inflammation in hDC-SIGN^{+}/SIGN-R1$^{-/-}$ mice

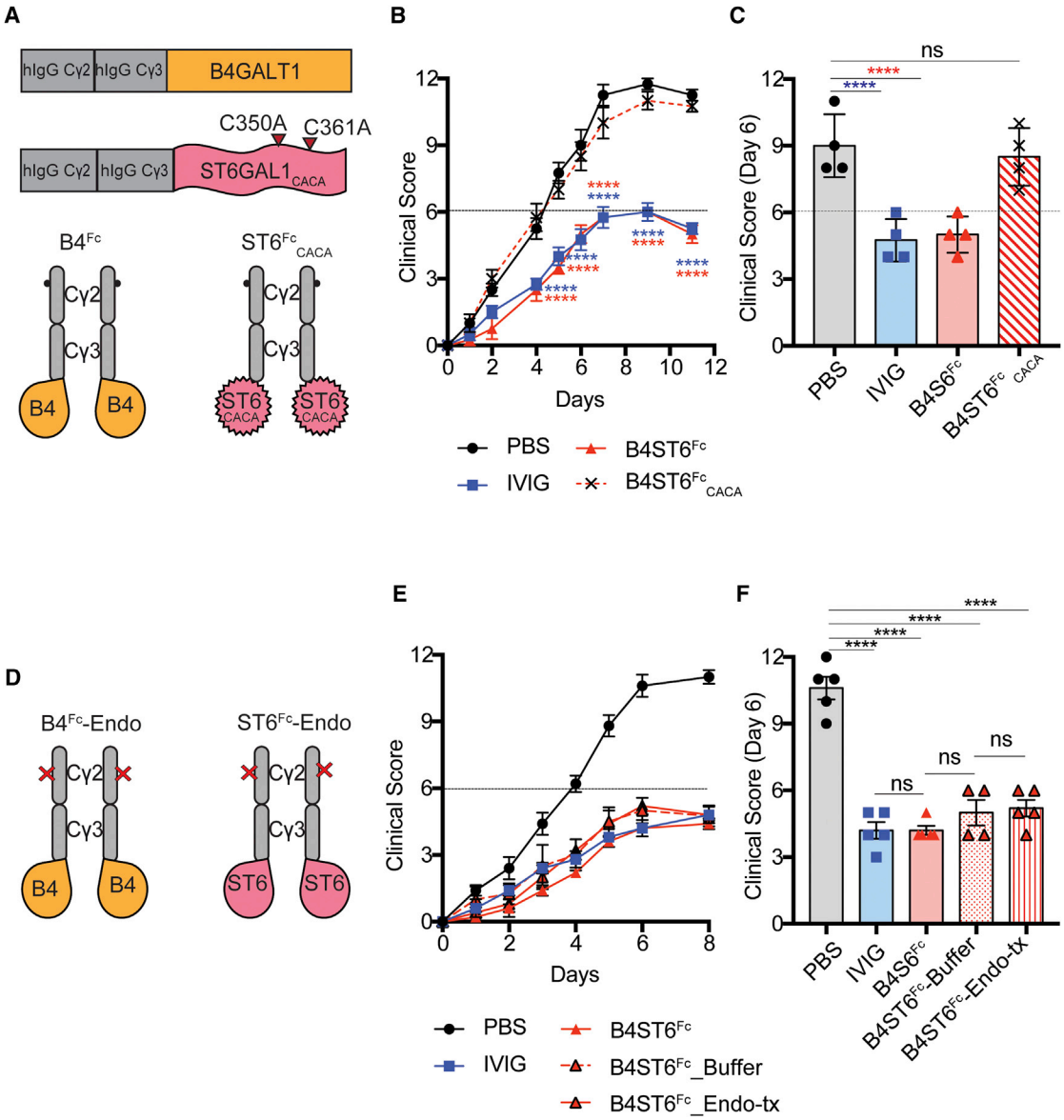

Figure 4. Enzymatic Requirements for *In Vivo* Sialylation

(A) B4GALT1 and enzymatically inactive ST6GAL1 (B4ST6$^{Fc}_{CACA}$).

(B) Clinical scores of mice given K/BxN sera and PBS (black circles), IVIG (blue squares), or B4ST6^{Fc} (red triangles) or B4ST6$^{Fc}_{CACA}$ (black crosses, red dotted line).

(C) Day 6 scores from (B) are shown.

(D) B4^{Fc} and ST6^{Fc} Fc glycan removal by EndoS (B4ST6Fc-Endo).

(E) Clinical scores of mice given K/BxN sera and PBS (black circles), IVIG (blue squares), B4ST6^{Fc} (red triangles), B4ST6^{Fc}-buffer (red triangle with black edge, red dotted line), or B4ST6^{Fc}-Endo (red triangle with black edge, red solid line).

(F) Day 6 scores from (E) are shown.

Means and standard deviation are plotted. Results are representative of at least two independent repeats. *$p < 0.05$, **$p < 0.005$, ****$p < 0.001$, ns, determined by two-way ANOVA followed by Tukey's test. See also Figures S3 and S4.

(Figure 3F). These results suggest that IVIG and *in vivo* sialylation suppress inflammation through similar pathways.

The shared receptors and pathways between IVIG and *in vivo* sialylation raised the possibility that the Fc glycans on the B4ST6^{Fc}, and not enzymatic activity, were responsible for anti-inflammatory activity. Therefore, we generated an enzymatically inactive ST6^{Fc} by mutating two enzymatic domain cysteine residues to alanine (C350A and C361A, ST6$^{Fc}_{CACA}$, Figure 4A [Meng et al., 2013]). B4ST6$^{Fc}_{CACA}$ was unable to transfer sialic acid to human IgG Fc *in vitro*, although galactosyltransferase activity remained intact (Figure S3E). B4ST6$^{Fc}_{CACA}$ did not reduce K/BxN-induced inflammation compared to IVIG

and B4ST6^{Fc} (Figures 4B and 4C). Next, B4^{Fc} and ST6^{Fc} were incubated with the IgG Fc-specific endoglycosidase EndoS to remove Fc glycans or with EndoS buffer only (B4ST6^{Fc}-Endo, B4ST6^{Fc}-Buffer; Figure 4D) (Collin and Olsén, 2001). Removal of the Fc glycan has been shown to ablate interactions of IgG and FcγRs and ablate IVIG anti-inflammatory activity (Allhorn et al., 2010; Benkhoucha et al., 2012; Kaneko et al., 2006b; Yang et al., 2010). B4ST6^{Fc}-Endo retained galactosyl- and sialyltransferase activity (Figure S3E) and was tested for anti-inflammatory activity *in vivo*. K/BxN-induced inflammation was attenuated by IVIG, B4ST6^{Fc}, B4ST6^{Fc}-Endo, and B4ST6^{Fc}-buffer (Figures 4E and 4F). These results demonstrate that transferase activity, and not Fc glycans on engineered enzymes, are required for suppression of inflammation *in vivo*.

Site-Specific Sialylation *In Vivo*

A potential undesirable side effect of *in vivo* sialylation may be off-target glycan modification. In general, low levels of sialic acid are found on IgG Fc glycans, as 5%–10% of total IgG in healthy individuals have sialylated Fc glycans. Most complex glycans are highly sialylated, limiting potential off-target effects of *in vivo* sialylation (Kaneko et al., 2006b; Youings et al., 1996). Nonetheless, we sought to examine toxicity and systemic glycosylation following B4ST6^{Fc} administration *in vivo*. The half-life of B4ST6^{Fc} in circulation was similar to human IgG1 Fc (10 and 8 days, respectively; Figures S4A–S4C), suggesting that the Fc portion of these molecules similarly controls serum half-life *in vivo*. We next examined the homeostatic impact of B4ST6^{Fc} 1 week and 2 months after administration (Figure S4D). No detrimental effect was noted on complete blood counts (CBCs). Serum glucose and calcium levels remained within normal range, while kidney and liver function was unaltered on comprehensive metabolic panel (CMP) analysis. The CBC and CMP analysis following PBS and B4ST6^{Fc}treatment suggested that of B4ST6^{Fc} is not toxic (Figure S4D). We next examined the glycosylation of IgG and total serum proteins 1 week and 2 months following administration of B4ST6^{Fc} (Figures S4E–S4H). Minimal changes in glycosylation were observed in B4ST6^{Fc}-treated animals compared to PBS-treated controls, suggesting that nominal off-target effects result from *in vivo* sialylation.

Because administration of both engineered enzymes was anti-inflammatory *in vivo* but did not notably alter serum IgG or protein glycosylation during homeostatic conditions, we sought to examine glycosylation during a site-specific inflammatory response. K/BxN sera was administered to mice that also received PBS, IVIG, or B4ST6^{Fc}. 7 days after treatment, we observed no differences in circulating IgG in PBS-, IVIG-, or B4ST6^{Fc}-treated mice (Figures 5A and 5B). We analyzed the glycosylation of IgG recovered from the paws of the treated animals. Intriguingly, we observed an increase in sialylation of IgG recovered from the paws of B4ST6^{Fc}-treated animals compared to IgG recovered from paws of K/BxN- and PBS- or IVIG- treated mice (Figures 5C and 5D). Next, NTN was induced in a panel of mice that received PBS, IVIG, or B4ST6^{Fc}, and the total N-linked glycosylation was examined. 7 days after disease induction, no differences in circulating IgG in PBS-, IVIG-, or B4ST6^{Fc}-treated mice were detected, consistent with our analyses on circulating glycoproteins (Figures 5E and 5F). However, we detected increases in sialylation of IgG recovered from the kidneys of B4ST6^{Fc}-treated animals compared to IgG recovered from circulation of PBS- or IVIG- treated mice (Figures 5G, 5H, and S5A). Sialylation of IgG recovered from the liver of B4ST6^{Fc}-treated animals in which NTN was induced demonstrated marked reduction compared to kidney-deposited IgG (Figure S5B). Immunoblot analysis of IgG purified from the serum (S) and kidney (K) of PBS-, IVIG-, or B4ST6^{Fc}-treated animals revealed measurable levels of mouse IgG in all samples, while human IgG Fc were only detectable in mice treated with IVIG, indicating our analysis of IgG glycans was restricted to endogenous mouse IgG Fc (Figure S5C). Further, macrophages in kidneys following of NTN- and PBS-, IVIG-, or B4ST6^{Fc}-treated WT animals, but not untreated controls, were positive for SIGN-R1^{+} (Figure S6A). SIGN-R1-staining was absent in NTN-induced SIGN-R1$^{-/-}$ mouse kidneys. hDC-SIGN^{+} macrophages were detected in kidneys of hDC-SIGN^{+}/SIGN-R1$^{-/-}$ mice following NTN induction (Figure S6B). Together, these results demonstrate that endogenous IgG at the site of inflammation is sialylated selectively by B4ST6^{Fc} in proximity to type II FcγR^{+} macrophages.

In Vivo Sialylation Requires Platelet Activation

Studies examining the activity of soluble ST6GAL1 implicated platelets as donors of CMP-SA, which is required for sialylation reactions (Jones et al., 2012; Jones et al., 2016; Lee et al., 2014). We therefore hypothesized that platelets also provided sugar-nucleotide donors for B4ST6^{Fc}. Indeed, CD41^{+} platelets were detected in the glomeruli of mouse kidneys in which NTN had been induced, but not in the glomeruli of untreated kidneys, consistent with previous studies demonstrating platelet recruitment to sites of inflammation (Figures 6A, 6B, and S7A [Boilard et al., 2010; Devi et al., 2010]). Further, CD41^{+} platelets in NTN-inflamed kidneys also expressed the platelet activation marker, CD62P (Figure 6B). Treatment with PBS, IVIG, or B4ST6^{Fc} during NTN-inflammation did not affect accumulation and activation of platelets (Figure 6B).

We next asked whether platelet activation was required for the anti-inflammatory activity of *in vivo* sialylation. Mice were given clopidogrel (10 mg/kg) daily 2 days prior to administration of K/BxN sera to prevent platelet activation by inhibiting the P2Y$_{12}$ subtype of the ADP receptor (Brown et al., 2015; Pucci et al., 2016). The mice also received PBS, IVIG, or B4ST6^{Fc}, and inflammation was monitored over the next several days. Clopidogrel treatment did not affect induced inflammation of PBS-treated animals (Figures 6C–6E). IVIG suppressed inflammation in the presence of clopidogrel (Figures 6C–6E). However, B4ST6^{Fc} was unable to attenuate inflammation when given coordinately with clopidogrel (Figures 6C–6E). Consistently, B4ST6^{Fc} was unable to attenuate K/BxN-induced inflammation when ozagrel, a thromboxane A2 synthesis inhibitor, or sulfinpyrazone, which reduces release of ADP and thromboxane, were administered (Figure S7B) (Loo et al., 1987; Underwood, 2006).

To extend these results, NTN was induced in mice that were administered clopidogrel (Figures 6F–6H) then received PBS, IVIG, or B4ST6^{Fc}. Importantly, these treatments did not affect

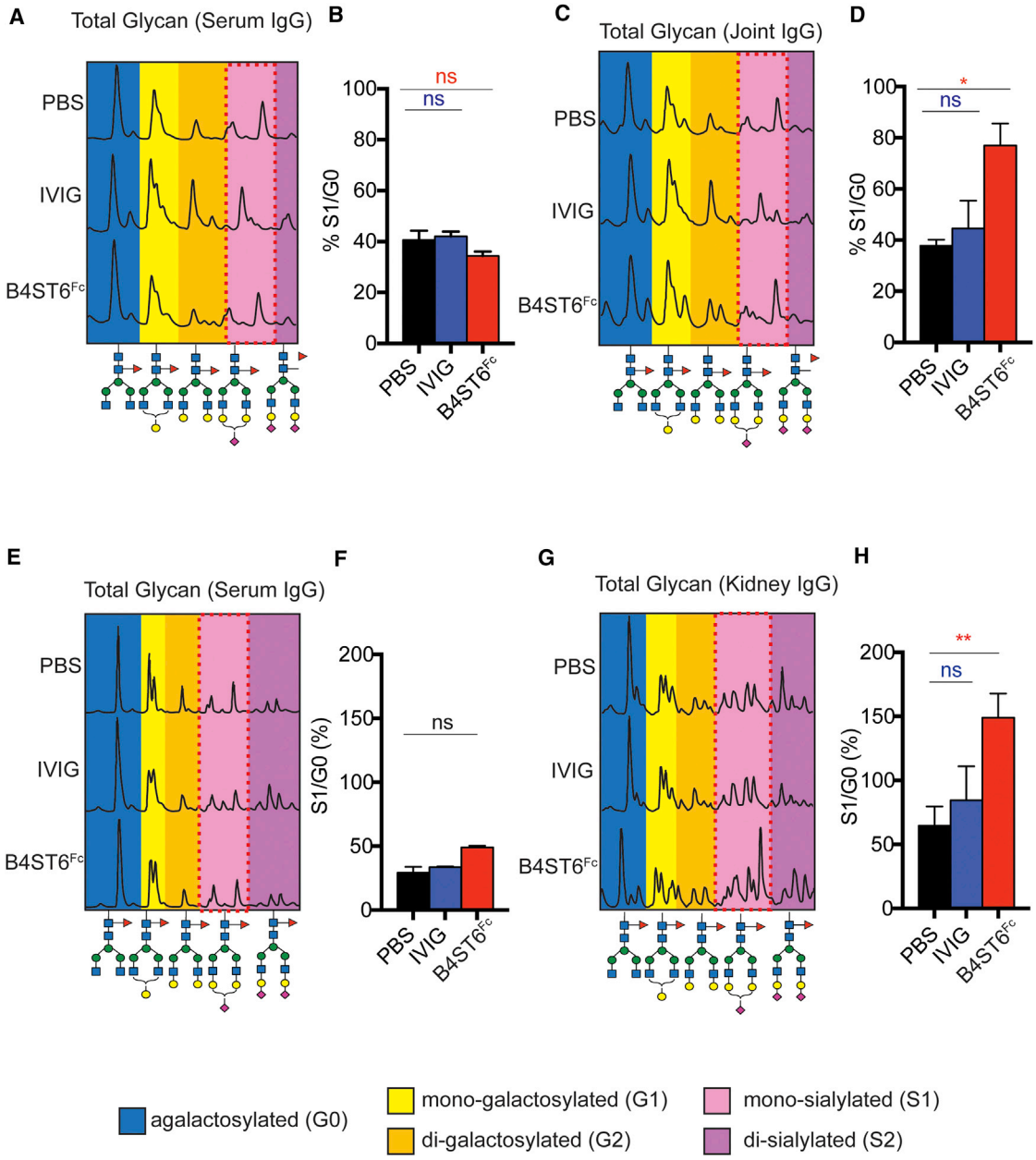

Figure 5. Characterizing *In Vivo* Sialylation during Autoimmune Inflammation

(A and B) (A) HPLC glycan traces and (B) ratios of monosialylated and agalactosylated glycans (S1/G0) of serum IgG after K/BxN and PBS, IVIG, or B4ST6^{Fc} treatment.

(C and D) (C) HPLC glycan traces and (D) ratios of monosialylated and agalactosylated glycans (S1/G0) of joint-deposited IgG after K/BxN and PBS, IVIG, or B4ST6^{Fc} treatment.

(E and F) (E) HPLC glycan traces and (F) ratios of monosialylated and agalactosylated glycans (S1/G0) from serum IgG of NTN-treated mice following administration of PBS, IVIG, or B4ST6^{Fc}.

(G and H) (G) HPLC glycan traces and (H) ratios of mono-sialylated and agalactosylated glycans (S1/G0) of kidney-deposited IgG of NTN-treated mice are shown. For (A), (C), (E), and (F), shading corresponds to retention time of terminal sugar (blue, G0; yellow, G1; orange, G2; pink, S1; purple, S2). Means and standard deviation are plotted. Results are representative of at least two independent repeats. **$p < 0.01$, ns, determined by two-way ANOVA followed by Tukey's test. See also Figure S5.

the anti-sheep IgG titers in the treated mice (Figure S7C). Induction of NTN caused kidney damage in clopidogrel and PBS-treated animals, as measured by BUN levels and survival (Figures 6F–6H). IVIG protected treated mice from kidney disease regardless of clopidogrel treatment (Figures 6F–6H). However, B4ST6^{Fc} was ineffective at attenuating disease when

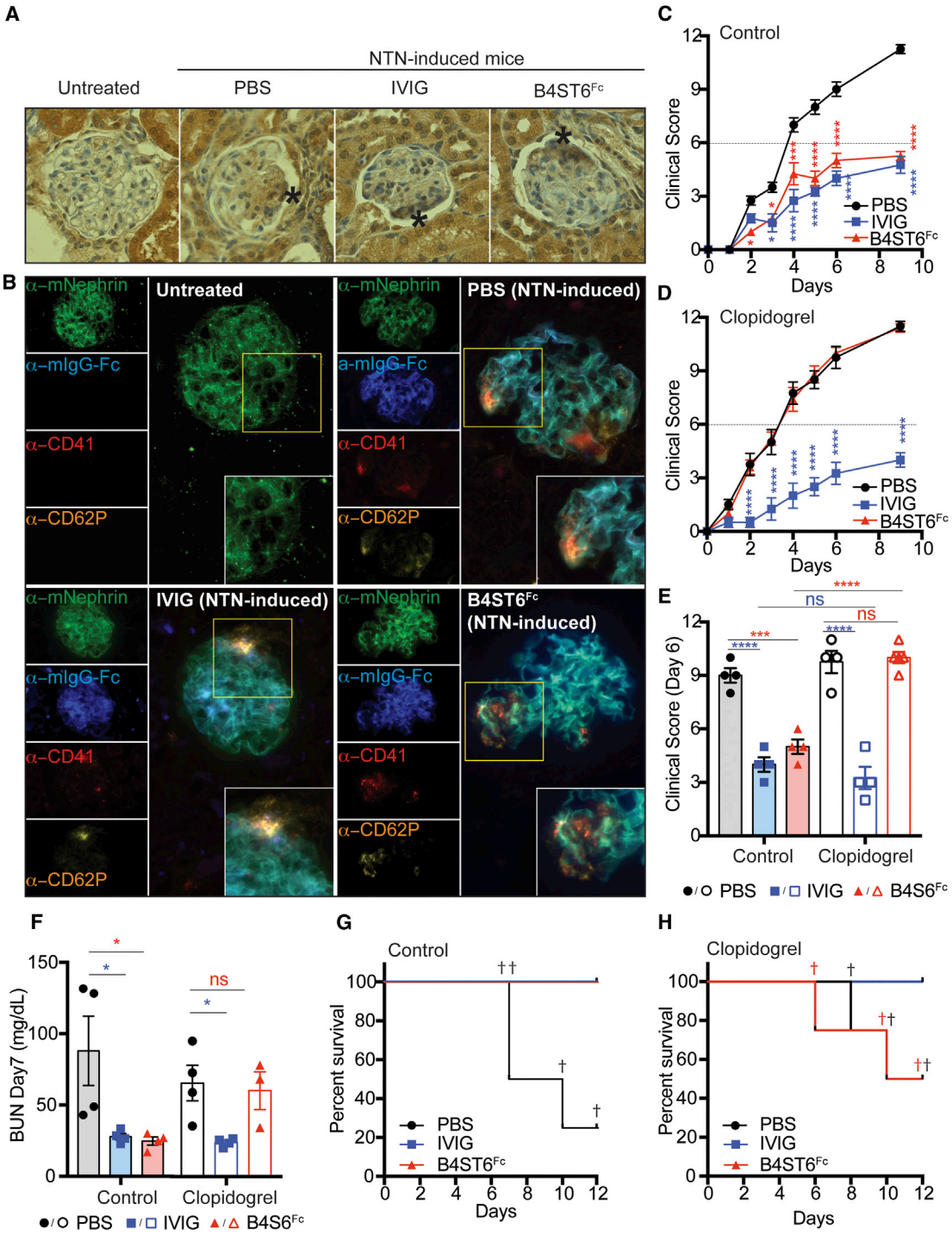

Figure 6. Platelet Activation and *In Vivo* Sialylation

(A) CD41-specific IHC in kidneys of untreated and day 7 NTN-induced mice following treatment with PBS, IVIG and B4ST6^{Fc}. Black asterisks indicate CD41^{+} platelet accumulation.

(B) Kidneys of untreated and day 7 NTN-treated mice following treatment with PBS, IVIG and B4ST6^{Fc} were examined for glomeruli (mNephrin, green), mouse IgG (blue), platelets (CD41, red), and activated platelets (CD62, yellow). Representative individual and overlaid images are shown.

(C and D) Clinical scores of control- and clopidogrel-treated mice given K/BxN sera and PBS (black circles), IVIG (blue squares), or B4ST6^{Fc} (red triangles).

(legend continued on next page)

given along with clopidogrel (Figures 6F and 6H). Together, these results demonstrate that the anti-inflammatory activity of B4ST6^{Fc}, but not IVIG, is dependent on platelet activation *in vivo*.

Next, we examined the glycosylation of IgG recovered from the paws of K/BxN- and clopidogrel-treated mice that also received PBS or B4ST6^{Fc}. Site-specific IgG sialylation was significantly reduced by clopidogrel treatment, further supporting a requirement for platelet activation during *in vivo* sialylation (Figures 7A and 7B). We next asked whether human platelets released sugar-nucleotide donors required for sialylation and collected platelet-enriched plasma (PRP) from healthy donors (Jones et al., 2016; Lee et al., 2014; Tan et al., 2016). Untreated platelets, thrombin-activated platelets (Thrombin+), or thrombin-activated clopidogrel-treated platelets were assayed for release of sialic acid- and galactose-nucleotide donors (CMP-SA, UDP-Gal). Indeed, human platelets released both sialic acid- and galactose-nucleotide donors upon activation, which was significantly inhibited by clopidogrel (Figures 7C and 7D).

A successful anti-inflammatory therapeutic is required to suppress ongoing inflammation. To determine whether *in vivo* sialylation was effective therapeutically, mice were treated with K/BxN sera and then given PBS, IVIG, or B4ST6^{Fc} on day 0 or day 3 after arthritis induction. IVIG and B4ST6^{Fc} were effective at reducing arthritis when administered on day 0 (Figures S7D and S7E). However, IVIG was unable to suppress induced arthritis when administered day 3 after disease induction (Figures 7E and 7F). Importantly, mice treated with B4ST6^{Fc} on day 3 exhibited significantly reduced inflammation on days 7 and 8 compared to IVIG- and PBS-treated groups (Figures 7E and 7F). These results reveal that B4ST6^{Fc} is able to effectively attenuate autoantibody-induced inflammation in a therapeutic fashion, which was unachievable with IVIG in this model (Bruhns et al., 2003).

DISCUSSION

This study explores modulation of IgG effector function by engineering antibody glycans *in vivo* as a novel means to attenuate autoantibody-mediated inflammation. Although the mechanisms regulating IgG glycosylation have not been fully elucidated, B cells, plasma cells, cytokine milieu, and extracellular glycosyltransferases likely influence IgG Fc glycoforms (Jones et al., 2012; Jones et al., 2016; Lee et al., 2014; Ohmi et al., 2016; Pfeifle et al., 2017; Wang et al., 2015). Indeed, the contribution of IgG glycosylation to infectious diseases and vaccines is increasingly appreciated (Lu et al., 2016; Wang et al., 2015; Wang et al., 2017).

The mechanisms governing the dose-dependent anti-inflammatory actions of IgG have been extensively debated (Clynes, 2007; Schwab and Nimmerjahn, 2013). Functional tests have shown that sialylation of IgG is responsible for IVIG anti-inflammatory activity *in vivo* (Fiebiger et al., 2015; Kaneko et al., 2006b; Ohmi et al., 2016; Schwab et al., 2012; Schwab et al., 2014; Washburn et al., 2015; Zhang et al., 2016). Generation of sialylated IgG Fcs is not trivial and has likely contributed to confusion in the literature. Indeed, contaminating LPS, Fc degradation, improper lectin-enrichment (Stadlmann et al., 2009), esoteric *in vitro* assays (Bayry et al., 2009), and heterogeneity of IVIG-Fab specificity have confounded results. ST6GAL1 can both attach and remove sialic acid, underscoring the importance of characterization of the sialylated material (Washburn et al., 2015). Of note, *in vivo* sialylation circumvents many technical issues of generating anti-inflammatory sialylated IgG.

Successful glycoengineering *in vivo* efforts have used bacterial-derived glycan-modifying enzymes (Albert et al., 2008; Xiao et al., 2016). The Streptococcal endoglycosidase, EndoS, attenuated IgG-mediated inflammation (Albert et al., 2008). Also, a *Vibrio cholerae* neuraminidase targeted to tumor glycocalixes improved ADCC (Xiao et al., 2016). While demonstrated the power of glycoengineering, repeated administration of these drugs may prove difficult because of immune responses targeting bacterial-derived enzymes. While it is possible that B4ST6^{Fc} will be targeted by the immune response, other human IgG Fc fusions have been well tolerated.

The potential for *in vivo* sialylation extends well beyond autoimmune and inflammatory conditions. Indeed, this approach may be applied to conditions currently treated by high-dose IVIG. Modulation of IgG sialylation could also be utilized to improve vaccine efficacy, as studies have reported that initial IgG generated following vaccination are sialylated, and these sialylated IgGs contribute to improved affinity maturation through a type II FcγR-dependent mechanism (Wang et al., 2015). Furthermore, *in vivo* sialylation may prove effective at truncating the activity of therapeutic IgG at defined intervals after treatment. Also, these glycosyltransferases could be further engineered, including increased FcRn affinity to extend serum half-life or increased/decreased receptor binding (Schlothauer et al., 2016).

We sought to exploit the functions of sialylation on IgG biology by fusing human glycosylation enzymes found in the *trans*-Golgi to IgG Fcs. Efficient sialylation *in vivo* required enzymes that attach galactose and sialic acid (Anthony et al., 2008a). This combination attenuated autoantibody-mediated inflammation in two distinct models *in vivo* by selectively sialylating IgG deposited at the site of inflammation. Administration of this enzyme combination does not appear to affect sialylation of IgG in circulation or that of other glycoproteins in circulation. This is likely due to platelets' release of galactose and sialic acid substrates only at sites of inflammation. Thus, *in vivo* sialylation is a novel and potent approach to attenuate harmful autoantibody-mediated inflammation through glycoengineering endogenous antibodies and converting them to anti-inflammatory mediators.

(E) Day 6 scores of (C) and (D) are shown.

(F–H) NTN was induced in control (F and G)- and clopidogrel (F and H)-treated animals and day 7 BUN levels (mg/dL) and survival were monitored.

Means and standard deviation are plotted. Results are representative of at least two independent repeats. *$p < 0.05$, ***$p < 0.005$, ****$p < 0.001$, ns, determined by two-way ANOVA followed by Tukey's test. See also Figures S5, S6, and S7.

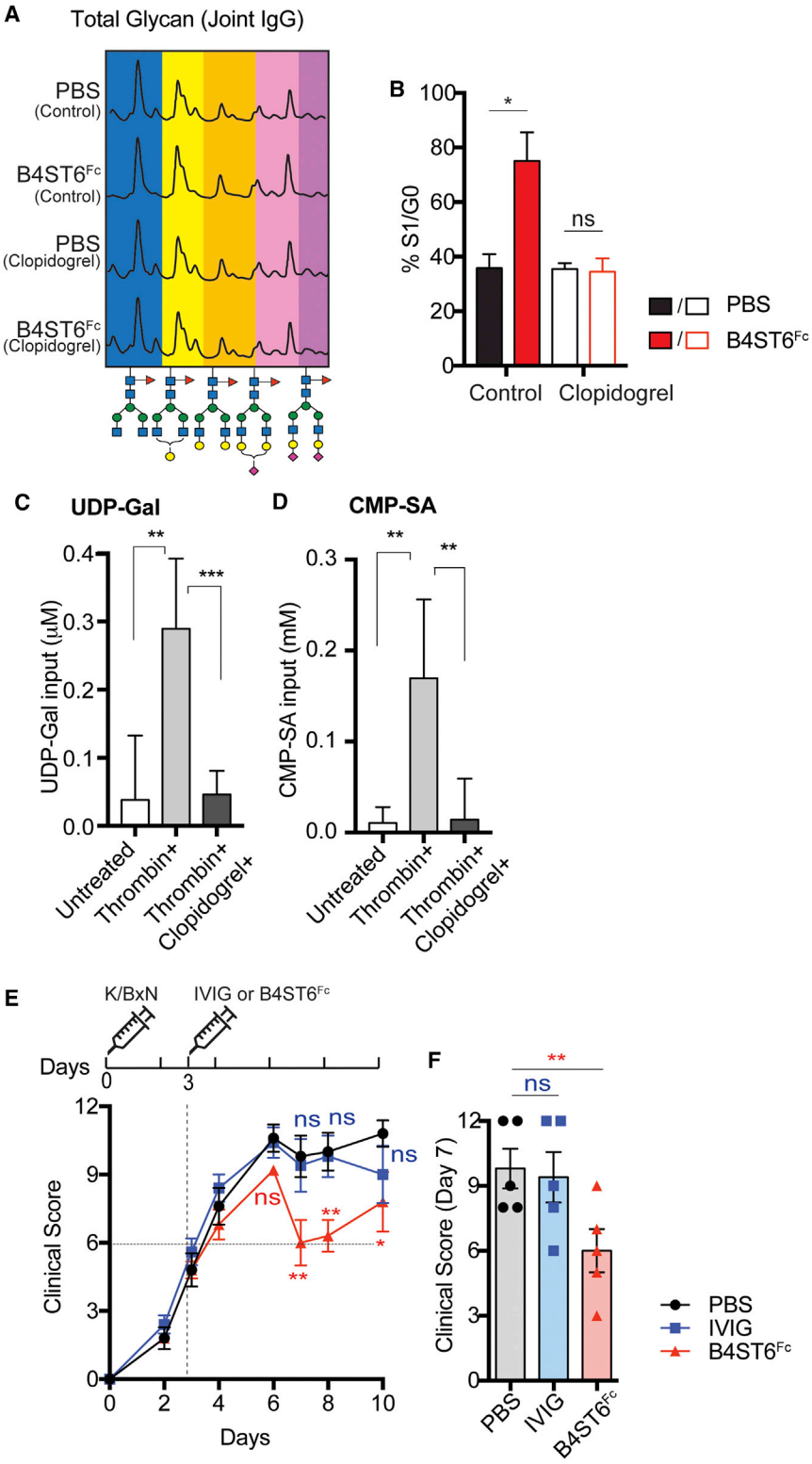

Figure 7. Therapeutic *In Vivo* Sialylation

(A) HPLC glycan traces of IgG recovered from joint after K/BxN and PBS or B4ST6^{Fc} treatment with or without clopidogrel.

(B) Ratios of monosialylated and agalactosylated glycans (S1/G0) from IgG described in (A).

(C and D) Human platelets were untreated, activated (Thrombin+), or activated after clopidogrel treatment (Thrombin+, Clopidogrel+), and assayed for UPD-Gal (C) and CMP-SA (D).

(E) Clinical scores of mice treated with K/BxN sera on day 0 and PBS (black circles), IVIG (blue squares), or B4ST6^{Fc} (red triangles) on day 3.

(F) Day 7 scores from (E) are shown.

Means and standard deviation are plotted. Results are representative of at least two independent repeats, ns, **$p < 0.01$, ***$p < 0.005$, ****$p < 0.001$, determined by two ANOVA followed by Tukey's test. See also Figure S7.

STAR★METHODS

Detailed methods are provided in the online version of this paper and include the following:

- KEY RESOURCES TABLE
- CONTACT FOR REAGENT AND RESOURCE SHARING
- EXPERIMENTAL MODEL AND SUBJECT DETAILS
  - Cell culture
  - In vivo animal studies
  - In vivo Platelet Inhibition Treatment
- METHOD DETAILS
  - Construction of glycosyltransferase fusions
  - In vitro glycosylation
  - Western and Lectin Blots
  - HPLC Glycan Analysis
  - K/BxN serum transfer
  - Nephrotoxic nephritis
  - ELISA
  - Kidney and joint IgG purification
  - Histology
  - Glomerulosclerosis and platelet infiltration
  - Platelet preparation
  - Quantification of UDP-Gal and CMP-SA
  - Serum Half-life Experiments
  - Blood testing
- QUANTIFICATION AND STATISTICAL ANALYSIS

SUPPLEMENTAL INFORMATION

Supplemental Information includes seven figures and one table and can be found with this article online at https://doi.org/10.1016/j.cell.2017.11.041.

AUTHOR CONTRIBUTIONS

M.K. and J.D.P. performed experiments, analyzed data, and wrote the manuscript. R.M.A. directed the studies and wrote the manuscript with M.K. and J.D.P.

ACKNOWLEDGMENTS

This work was supported by grants from NIAMS/NIH (DP2AR068272), the Lupus Research Alliance, and the MGH H.M. Goodman Fellowship to R.M.A. The authors are grateful to J. Paulson for providing anti-ST6GAL1 anti-sera; J. Ravetch for providing K/BxN sera; H. Meade for providing ST6GAL1; M.E. Conroy; J.W. Griffith; R. Rahimi; C. Sokol for clinical expertise; and K. Jeffrey, F. Wermeling, T. Mayadas, M. Pittet, K.T. Shade, E.E. Martinez, M.E. Conroy, T. Means, and A. Luster for constructive comments and careful reading of this manuscript.

Received: July 25, 2017
Revised: October 20, 2017
Accepted: November 21, 2017
Published: December 21, 2017

REFERENCES

Ackerman, M.E., Crispin, M., Yu, X., Baruah, K., Boesch, A.W., Harvey, D.J., Dugast, A.S., Heizen, E.L., Ercan, A., Choi, I., et al. (2013). Natural variation in Fc glycosylation of HIV-specific antibodies impacts antiviral activity. J. Clin. Invest. *123*, 2183–2192.

Aigouy, B., and Mirouse, V. (2013). ScientiFig: a tool to build publication-ready scientific figures. Nat. Methods *10*, 1048.

Albert, H., Collin, M., Dudziak, D., Ravetch, J.V., and Nimmerjahn, F. (2008). In vivo enzymatic modulation of IgG glycosylation inhibits autoimmune disease in an IgG subclass-dependent manner. Proc. Natl. Acad. Sci. USA *105*, 15005–15009.

Allhorn, M., Briceño, J.G., Baudino, L., Lood, C., Olsson, M.L., Izui, S., and Collin, M. (2010). The IgG-specific endoglycosidase EndoS inhibits both cellular and complement-mediated autoimmune hemolysis. Blood *115*, 5080–5088.

Anthony, R.M., Nimmerjahn, F., Ashline, D.J., Reinhold, V.N., Paulson, J.C., and Ravetch, J.V. (2008a). Recapitulation of IVIG anti-inflammatory activity with a recombinant IgG Fc. Science *320*, 373–376.

Anthony, R.M., Wermeling, F., Karlsson, M.C., and Ravetch, J.V. (2008b). Identification of a receptor required for the anti-inflammatory activity of IVIG. Proc. Natl. Acad. Sci. USA *105*, 19571–19578.

Anthony, R.M., Kobayashi, T., Wermeling, F., and Ravetch, J.V. (2011). Intravenous gammaglobulin suppresses inflammation through a novel T(H)2 pathway. Nature *475*, 110–113.

Arnold, J.N., Wormald, M.R., Sim, R.B., Rudd, P.M., and Dwek, R.A. (2007). The impact of glycosylation on the biological function and structure of human immunoglobulins. Annu. Rev. Immunol. *25*, 21–50.

Bayry, J., Bansal, K., Kazatchkine, M.D., and Kaveri, S.V. (2009). DC-SIGN and alpha2,6-sialylated IgG Fc interaction is dispensable for the anti-inflammatory activity of IVIg on human dendritic cells. Proc. Natl. Acad. Sci. U. S. A. *106*, E24; author reply E25.

Benkhoucha, M., Molnarfi, N., Santiago-Raber, M.L., Weber, M.S., Merkler, D., Collin, M., and Lalive, P.H. (2012). IgG glycan hydrolysis by EndoS inhibits experimental autoimmune encephalomyelitis. J. Neuroinflammation *9*, 209.

Boilard, E., Nigrovic, P.A., Larabee, K., Watts, G.F., Coblyn, J.S., Weinblatt, M.E., Massarotti, E.M., Remold-O'Donnell, E., Farndale, R.W., Ware, J., and Lee, D.M. (2010). Platelets amplify inflammation in arthritis via collagen-dependent microparticle production. Science *327*, 580–583.

Brown, D.G., Wilkerson, E.C., and Love, W.E. (2015). A review of traditional and novel oral anticoagulant and antiplatelet therapy for dermatologists and dermatologic surgeons. J. Am. Acad. Dermatol. *72*, 524–534.

Bruhns, P., Samuelsson, A., Pollard, J.W., and Ravetch, J.V. (2003). Colony-stimulating factor-1-dependent macrophages are responsible for IVIG protection in antibody-induced autoimmune disease. Immunity *18*, 573–581.

Campbell, I.K., Miescher, S., Branch, D.R., Mott, P.J., Lazarus, A.H., Han, D., Maraskovsky, E., Zuercher, A.W., Neschadim, A., Leontyev, D., et al. (2014). Therapeutic effect of IVIG on inflammatory arthritis in mice is dependent on the Fc portion and independent of sialylation or basophils. J. Immunol. *192*, 5031–5038.

Chung, A.W., Ghebremichael, M., Robinson, H., Brown, E., Choi, I., Lane, S., Dugast, A.S., Schoen, M.K., Rolland, M., Suscovich, T.J., et al. (2014). Polyfunctional Fc-effector profiles mediated by IgG subclass selection distinguish RV144 and VAX003 vaccines. Sci. Transl. Med. *6*, 228ra38.

Clynes, R. (2007). Protective mechanisms of IVIG. Curr. Opin. Immunol. *19*, 646–651.

Collin, M., and Olsén, A. (2001). EndoS, a novel secreted protein from Streptococcus pyogenes with endoglycosidase activity on human IgG. EMBO J. *20*, 3046–3055.

Davies, J., Jiang, L., Pan, L.Z., LaBarre, M.J., Anderson, D., and Reff, M. (2001). Expression of GnTIII in a recombinant anti-CD20 CHO production cell line: Expression of antibodies with altered glycoforms leads to an increase in ADCC through higher affinity for FC gamma RIII. Biotechnol. Bioeng. *74*, 288–294.

Debré, M., Bonnet, M.C., Fridman, W.H., Carosella, E., Philippe, N., Reinert, P., Vilmer, E., Kaplan, C., Teillaud, J.L., and Griscelli, C. (1993). Infusion of Fc gamma fragments for treatment of children with acute immune thrombocytopenic purpura. Lancet *342*, 945–949.

Devi, S., Kuligowski, M.P., Kwan, R.Y., Westein, E., Jackson, S.P., Kitching, A.R., and Hickey, M.J. (2010). Platelet recruitment to the inflamed glomerulus occurs via an alphaIIbbeta3/GPVI-dependent pathway. Am. J. Pathol. *177*, 1131–1142.

Ferrara, C., Grau, S., Jäger, C., Sondermann, P., Brünker, P., Waldhauer, I., Hennig, M., Ruf, A., Rufer, A.C., Stihle, M., et al. (2011). Unique carbohydrate-carbohydrate interactions are required for high affinity binding between FcgammaRIII and antibodies lacking core fucose. Proc. Natl. Acad. Sci. USA *108*, 12669–12674.

Fiebiger, B.M., Maamary, J., Pincetic, A., and Ravetch, J.V. (2015). Protection in antibody- and T cell-mediated autoimmune diseases by antiinflammatory IgG Fcs requires type II FcRs. Proc. Natl. Acad. Sci. USA *112*, E2385–E2394.

Franklin, E.C. (1975). Structure and function of immunoglobulins. Acta Endocrinol. Suppl. (Copenh.) *194*, 77–95.

Hansen, R.J., and Balthasar, J.P. (2002). Intravenous immunoglobulin mediates an increase in anti-platelet antibody clearance via the FcRn receptor. Thromb. Haemost. *88*, 898–899.

Huber, R., Deisenhofer, J., Colman, P.M., Matsushima, M., and Palm, W. (1976). Crystallographic structure studies of an IgG molecule and an Fc fragment. Nature *264*, 415–420.

Imbach, P., Barandun, S., d'Apuzzo, V., Baumgartner, C., Hirt, A., Morell, A., Rossi, E., Schöni, M., Vest, M., and Wagner, H.P. (1981). High-dose intravenous gammaglobulin for idiopathic thrombocytopenic purpura in childhood. Lancet *1*, 1228–1231.

Ishitsuka, Y., Moriuchi, H., Isohama, Y., Tokunaga, H., Hatamoto, K., Kurita, S., Irikura, M., Iyama, K., and Irie, T. (2009). A selective thromboxane A2 (TXA2) synthase inhibitor, ozagrel, attenuates lung injury and decreases monocyte chemoattractant protein-1 and interleukin-8 mRNA expression in oleic acid-induced lung injury in guinea pigs. J. Pharmacol. Sci. *111*, 211–215.

Jefferis, R. (2005). Glycosylation of recombinant antibody therapeutics. Biotechnol. Prog. *21*, 11–16.

Jefferis, R. (2009a). Glycosylation as a strategy to improve antibody-based therapeutics. Nat. Rev. Drug Discov. *8*, 226–234.

Jefferis, R. (2009b). Glycosylation of antibody therapeutics: optimisation for purpose. Methods Mol. Biol. *483*, 223–238.

Jones, M.B., Nasirikenari, M., Lugade, A.A., Thanavala, Y., and Lau, J.T. (2012). Anti-inflammatory IgG production requires functional P1 promoter in β-galactoside α2,6-sialyltransferase 1 (ST6Gal-1) gene. J. Biol. Chem. *287*, 15365–15370.

Jones, M.B., Oswald, D.M., Joshi, S., Whiteheart, S.W., Orlando, R., and Cobb, B.A. (2016). B-cell-independent sialylation of IgG. Proc. Natl. Acad. Sci. USA *113*, 7207–7212.

Kalcheva, I., Elliott, R.W., Dalziel, M., and Lau, J.T. (1997). The gene encoding beta-galactoside alpha2,6-sialyltransferase maps to mouse chromosome 16. Mamm. Genome *8*, 619–620.

Kaneko, Y., Nimmerjahn, F., Madaio, M.P., and Ravetch, J.V. (2006a). Pathology and protection in nephrotoxic nephritis is determined by selective engagement of specific Fc receptors. J. Exp. Med. *203*, 789–797.

Kaneko, Y., Nimmerjahn, F., and Ravetch, J.V. (2006b). Anti-inflammatory activity of immunoglobulin G resulting from Fc sialylation. Science *313*, 670–673.

Kang, Y.S., Kim, J.Y., Bruening, S.A., Pack, M., Charalambous, A., Pritsker, A., Moran, T.M., Loeffler, J.M., Steinman, R.M., and Park, C.G. (2004). The C-type lectin SIGN-R1 mediates uptake of the capsular polysaccharide of Streptococcus pneumoniae in the marginal zone of mouse spleen. Proc. Natl. Acad. Sci. USA *101*, 215–220.

Korganow, A.S., Ji, H., Mangialaio, S., Duchatelle, V., Pelanda, R., Martin, T., Degott, C., Kikutani, H., Rajewsky, K., Pasquali, J.L., et al. (1999). From systemic T cell self-reactivity to organ-specific autoimmune disease via immunoglobulins. Immunity *10*, 451–461.

Kouskoff, V., Korganow, A.S., Duchatelle, V., Degott, C., Benoist, C., and Mathis, D. (1996). Organ-specific disease provoked by systemic autoimmunity. Cell *87*, 811–822.

Lanoue, A., Clatworthy, M.R., Smith, P., Green, S., Townsend, M.J., Jolin, H.E., Smith, K.G., Fallon, P.G., and McKenzie, A.N. (2004). SIGN-R1 contributes to protection against lethal pneumococcal infection in mice. J. Exp. Med. *200*, 1383–1393.

Lee, M.M., Nasirikenari, M., Manhardt, C.T., Ashline, D.J., Hanneman, A.J., Reinhold, V.N., and Lau, J.T. (2014). Platelets support extracellular sialylation by supplying the sugar donor substrate. J. Biol. Chem. *289*, 8742–8748.

Lerner, R.A., Glassock, R.J., and Dixon, F.J. (1967). The role of anti-glomerular basement membrane antibody in the pathogenesis of human glomerulonephritis. J. Exp. Med. *126*, 989–1004.

Li, N., Zhao, M., Hilario-Vargas, J., Prisayanh, P., Warren, S., Diaz, L.A., Roopenian, D.C., and Liu, Z. (2005). Complete FcRn dependence for intravenous Ig therapy in autoimmune skin blistering diseases. J. Clin. Invest. *115*, 3440–3450.

Li, T., DiLillo, D.J., Bournazos, S., Giddens, J.P., Ravetch, J.V., and Wang, L.X. (2017). Modulating IgG effector function by Fc glycan engineering. Proc. Natl. Acad. Sci. USA *114*, 3485–3490.

Loo, M.H., Egan, D., Vaughan, E.D., Jr., Marion, D., Felsen, D., and Weisman, S. (1987). The effect of the thromboxane A2 synthesis inhibitor OKY-046 on renal function in rabbits following release of unilateral ureteral obstruction. J. Urol. *137*, 571–576.

Lu, L.L., Chung, A.W., Rosebrock, T.R., Ghebremichael, M., Yu, W.H., Grace, P.S., Schoen, M.K., Tafesse, F., Martin, C., Leung, V., et al. (2016). A Functional Role for Antibodies in Tuberculosis. Cell *167*, 433–443.

Meng, L., Forouhar, F., Thieker, D., Gao, Z., Ramiah, A., Moniz, H., Xiang, Y., Seetharaman, J., Milaninia, S., Su, M., et al. (2013). Enzymatic basis for N-glycan sialylation: structure of rat α2,6-sialyltransferase (ST6GAL1) reveals conserved and unique features for glycan sialylation. J. Biol. Chem. *288*, 34680–34698.

Natsume, A., Wakitani, M., Yamane-Ohnuki, N., Shoji-Hosaka, E., Niwa, R., Uchida, K., Satoh, M., and Shitara, K. (2005). Fucose removal from complex-type oligosaccharide enhances the antibody-dependent cellular cytotoxicity of single-gene-encoded antibody comprising a single-chain antibody linked the antibody constant region. J. Immunol. Methods *306*, 93–103.

Negi, V.S., Elluru, S., Sibéril, S., Graff-Dubois, S., Mouthon, L., Kazatchkine, M.D., Lacroix-Desmazes, S., Bayry, J., and Kaveri, S.V. (2007). Intravenous immunoglobulin: an update on the clinical use and mechanisms of action. J. Clin. Immunol. *27*, 233–245.

Nimmerjahn, F., and Ravetch, J.V. (2008a). Anti-inflammatory actions of intravenous immunoglobulin. Annu. Rev. Immunol. *26*, 513–533.

Nimmerjahn, F., and Ravetch, J.V. (2008b). Fcgamma receptors as regulators of immune responses. Nat. Rev. Immunol. *8*, 34–47.

Nimmerjahn, F., Gordan, S., and Lux, A. (2015). FcγR dependent mechanisms of cytotoxic, agonistic, and neutralizing antibody activities. Trends Immunol. *36*, 325–336.

Ohmi, Y., Ise, W., Harazono, A., Takakura, D., Fukuyama, H., Baba, Y., Narazaki, M., Shoda, H., Takahashi, N., Ohkawa, Y., et al. (2016). Sialylation converts arthritogenic IgG into inhibitors of collagen-induced arthritis. Nat. Commun. *7*, 11205.

Okazaki, A., Shoji-Hosaka, E., Nakamura, K., Wakitani, M., Uchida, K., Kakita, S., Tsumoto, K., Kumagai, I., and Shitara, K. (2004). Fucose depletion from human IgG1 oligosaccharide enhances binding enthalpy and association rate between IgG1 and FcgammaRIIIa. J. Mol. Biol. *336*, 1239–1249.

Pfeifle, R., Rothe, T., Ipseiz, N., Scherer, H.U., Culemann, S., Harre, U., Ackermann, J.A., Seefried, M., Kleyer, A., Uderhardt, S., et al. (2017). Regulation of autoantibody activity by the IL-23-TH17 axis determines the onset of autoimmune disease. Nat. Immunol. *18*, 104–113.

Pincetic, A., Bournazos, S., DiLillo, D.J., Maamary, J., Wang, T.T., Dahan, R., Fiebiger, B.M., and Ravetch, J.V. (2014). Type I and type II Fc receptors regulate innate and adaptive immunity. Nat. Immunol. *15*, 707–716.

Pucci, F., Rickelt, S., Newton, A.P., Garris, C., Nunes, E., Evavold, C., Pfirschke, C., Engblom, C., Mino-Kenudson, M., Hynes, R.O., et al. (2016).

PF4 Promotes Platelet Production and Lung Cancer Growth. Cell Rep. *17*, 1764–1772.

Raeder, E.A., Verrier, R.L., and Lown, B. (1982). Effects of sulfinpyrazone on ventricular vulnerability in the normal and the ischemic heart. Am. J. Cardiol. *50*, 271–275.

Samuelsson, A., Towers, T.L., and Ravetch, J.V. (2001). Anti-inflammatory activity of IVIG mediated through the inhibitory Fc receptor. Science *291*, 484–486.

Scallon, B.J., Tam, S.H., McCarthy, S.G., Cai, A.N., and Raju, T.S. (2007). Higher levels of sialylated Fc glycans in immunoglobulin G molecules can adversely impact functionality. Mol. Immunol. *44*, 1524–1534.

Schlothauer, T., Herter, S., Koller, C.F., Grau-Richards, S., Steinhart, V., Spick, C., Kubbies, M., Klein, C., Umaña, P., and Mössner, E. (2016). Novel human IgG1 and IgG4 Fc-engineered antibodies with completely abolished immune effector functions. Protein Eng. Des. Sel. *29*, 457–466.

Schrijver, G., Bogman, M.J., Assmann, K.J., de Waal, R.M., Robben, H.C., van Gasteren, H., and Koene, R.A. (1990). Anti-GBM nephritis in the mouse: role of granulocytes in the heterologous phase. Kidney Int. *38*, 86–95.

Schwab, I., and Nimmerjahn, F. (2013). Intravenous immunoglobulin therapy: how does IgG modulate the immune system? Nat. Rev. Immunol. *13*, 176–189.

Schwab, I., and Nimmerjahn, F. (2014). Role of sialylation in the anti-inflammatory activity of intravenous immunoglobulin - $F(ab')_2$ versus Fc sialylation. Clin. Exp. Immunol. *178* (*Suppl 1*), 97–99.

Schwab, I., Biburger, M., Krönke, G., Schett, G., and Nimmerjahn, F. (2012). IVIg-mediated amelioration of ITP in mice is dependent on sialic acid and SIGNR1. Eur. J. Immunol. *42*, 826–830.

Schwab, I., Mihai, S., Seeling, M., Kasperkiewicz, M., Ludwig, R.J., and Nimmerjahn, F. (2014). Broad requirement for terminal sialic acid residues and FcγRIIB for the preventive and therapeutic activity of intravenous immunoglobulins in vivo. Eur. J. Immunol. *44*, 1444–1453.

Schwarzenberger, C., Sradnick, J., Lerea, K.M., Goligorsky, M.S., Nieswandt, B., Hugo, C.P., and Hohenstein, B. (2015). Platelets are relevant mediators of renal injury induced by primary endothelial lesions. Am. J. Physiol. Renal Physiol. *308*, F1238–F1246.

Shields, R.L., Lai, J., Keck, R., O'Connell, L.Y., Hong, K., Meng, Y.G., Weikert, S.H., and Presta, L.G. (2002). Lack of fucose on human IgG1 N-linked oligosaccharide improves binding to human Fcgamma RIII and antibody-dependent cellular toxicity. J. Biol. Chem. *277*, 26733–26740.

Stadlmann, J., Weber, A., Pabst, M., Anderle, H., Kunert, R., Ehrlich, H.J., Peter Schwarz, H., and Altmann, F. (2009). A close look at human IgG sialylation and subclass distribution after lectin fractionation. Proteomics *9*, 4143–4153.

Sugimoto, I., Futakawa, S., Oka, R., Ogawa, K., Marth, J.D., Miyoshi, E., Taniguchi, N., Hashimoto, Y., and Kitazume, S. (2007). Beta-galactoside alpha2,6-sialyltransferase I cleavage by BACE1 enhances the sialylation of soluble glycoproteins. A novel regulatory mechanism for alpha2,6-sialylation. J. Biol. Chem. *282*, 34896–34903.

Tackenberg, B., Jelcic, I., Baerenwaldt, A., Oertel, W.H., Sommer, N., Nimmerjahn, F., and Lünemann, J.D. (2009). Impaired inhibitory Fcgamma receptor IIB expression on B cells in chronic inflammatory demyelinating polyneuropathy. Proc. Natl. Acad. Sci. USA *106*, 4788–4792.

Tackenberg, B., Nimmerjahn, F., and Lünemann, J.D. (2010). Mechanisms of IVIG efficacy in chronic inflammatory demyelinating polyneuropathy. J. Clin. Immunol. *30* (*Suppl 1*), S65–S69.

Tan, M., Yan, H.B., Li, J.N., Li, W.K., Fu, Y.Y., Chen, W., and Zhou, Z. (2016). Thrombin Stimulated Platelet-Derived Exosomes Inhibit Platelet-Derived Growth Factor Receptor-Beta Expression in Vascular Smooth Muscle Cells. Cell. Physiol. Biochem. *38*, 2348–2365.

Tuominen, V.J., Ruotoistenmäki, S., Viitanen, A., Jumppanen, M., and Isola, J. (2010). ImmunoRatio: a publicly available web application for quantitative image analysis of estrogen receptor (ER), progesterone receptor (PR), and Ki-67. Breast Cancer Res. *12*, R56.

Underwood, M. (2006). Diagnosis and management of gout. BMJ *332*, 1315–1319.

Wang, X., Vertino, A., Eddy, R.L., Byers, M.G., Jani-Sait, S.N., Shows, T.B., and Lau, J.T. (1993). Chromosome mapping and organization of the human beta-galactoside alpha 2,6-sialyltransferase gene. Differential and cell-type specific usage of upstream exon sequences in B-lymphoblastoid cells. J. Biol. Chem. *268*, 4355–4361.

Wang, T.T., Maamary, J., Tan, G.S., Bournazos, S., Davis, C.W., Krammer, F., Schlesinger, S.J., Palese, P., Ahmed, R., and Ravetch, J.V. (2015). Anti-HA Glycoforms Drive B Cell Affinity Selection and Determine Influenza Vaccine Efficacy. Cell *162*, 160–169.

Wang, T.T., Sewatanon, J., Memoli, M.J., Wrammert, J., Bournazos, S., Bhaumik, S.K., Pinsky, B.A., Chokephaibulkit, K., Onlamoon, N., Pattanapanyasat, K., et al. (2017). IgG antibodies to dengue enhanced for FcγRIIIA binding determine disease severity. Science *355*, 395–398.

Washburn, N., Schwab, I., Ortiz, D., Bhatnagar, N., Lansing, J.C., Medeiros, A., Tyler, S., Mekala, D., Cochran, E., Sarvaiya, H., et al. (2015). Controlled tetra-Fc sialylation of IVIg results in a drug candidate with consistent enhanced anti-inflammatory activity. Proc. Natl. Acad. Sci. USA *112*, E1297–E1306.

Woodard-Grice, A.V., McBrayer, A.C., Wakefield, J.K., Zhuo, Y., and Bellis, S.L. (2008). Proteolytic shedding of ST6Gal-I by BACE1 regulates the glycosylation and function of alpha4beta1 integrins. J. Biol. Chem. *283*, 26364–26373.

Xiao, H., Woods, E.C., Vukojicic, P., and Bertozzi, C.R. (2016). Precision glycocalyx editing as a strategy for cancer immunotherapy. Proc. Natl. Acad. Sci. USA *113*, 10304–10309.

Yang, R., Otten, M.A., Hellmark, T., Collin, M., Björck, L., Zhao, M.H., Daha, M.R., and Segelmark, M. (2010). Successful treatment of experimental glomerulonephritis with IdeS and EndoS, IgG-degrading streptococcal enzymes. Nephrol. Dial. Transplant. *25*, 2479–2486.

Youings, A., Chang, S.C., Dwek, R.A., and Scragg, I.G. (1996). Site-specific glycosylation of human immunoglobulin G is altered in four rheumatoid arthritis patients. Biochem. J. *314*, 621–630.

Zhang, G., Massaad, C.A., Gao, T., Pillai, L., Bogdanova, N., Ghauri, S., and Sheikh, K.A. (2016). Sialylated intravenous immunoglobulin suppress anti-ganglioside antibody mediated nerve injury. Exp. Neurol. *282*, 49–55.

STAR★METHODS

KEY RESOURCES TABLE

REAGENT or RESOURCE	SOURCE	IDENTIFIER
Antibodies		
Anti-human IgG-HRP	Promega	Cat#: W4031
Anti-human B4GALT1	Sigma-Aldrich	Cat#: HPA010807
Anti-rabbit IgG-HRP	Promega	Cat#: W4011
Anti-mouse IgG-Fc-HRP	Bethyl Laboratories	Cat#: A90-131A
Anti-human ST6GAL1	J. Paulson	N/A
Anti-human IgG-Fc	Bethyl Laboratories	Cat#: A80-104A
Sheep IgG	BioRad	Cat#: PSP01
PE anti-mouse/rat CD62P	Biolegend	Cat#: 148305
APC anti-mouse CD41 Antibody	Biolegend	Cat#: 133913
Mouse nephrin antibody	R & D systems	Cat#: AF3159
DyLight 405 AffiniPure Rabbit Anti-Mouse IgG, Fcγ fragment specific	Jackson ImmunoResearch	Cat#: 315-475-008
Alexa Fluor 488 AffiniPure Donkey Anti-Goat IgG (H+L)	Jackson ImmunoResearch	Cat#: 705-545-003
Alexa Fluor 647 anti-SIGN-R1 (CD209b)	eBioscience	Cat#: 51-2093-82
Alexa Fluor 647 anti-human CD209 (DC-SIGN)	Biolegend	Cat#: 330112
PE anti-mouse F4/80	Biolegend	Cat#: 123110
Chemicals, Peptides, and Recombinant Proteins		
pcDNA3.4 TOPO TA Cloning Kit	Thermo Fisher	Cat#: A14697
Expi293 Expression System Kit	Thermo Fisher	Cat#: A14635
Pierce Protein G Plus Agarose	Thermo Fisher	Cat#: 22852B
Sialidase A	ProZyme	Cat#: GK80040
β1-4 Galactosidase S	New England Biolab	Cat#: P0745L
UDP-α-D-Galactose, Disodium Salt	Millipre Sigma	Cat#: 670111 CAS#: 137868-52-1
CMP-Sialic acid (Cytidine-5′-monophospho-N-acetylneuraminic Acid Disodium Salt)	Nacalai USA	Cat#: 10432-24
Pierce Protein-Free (TBS) Blocking Buffer	Thermo Fisher	Cat#: 37570
Biotinylated Sambucus Nigra Lectin (SNA)	Vector Laboratories	Cat#: B-1305
Biotinylated Erythrina Cristagalli Lectin (ECL)	Vector Laboratories	Cat#: B-1145
PNGase F	New England Biolab	Cat#: P0704L
Endo S	New England Biolab	Cat#: P0741L
GlykoClean G Cartridges	ProZyme	Cat#: GC250
GlykoClean S-plus Cartridges	ProZyme	Cat#: GC210
Anthranilamide (2-AB)	Sigma-Aldrich	Cat#: A89804
NTS (Sheep Anti-Rat Glomeruli (Anti-GBM) Serum)	Probetex	Cat#: PTX001-S
TMB Substrate	Biolegend	Cat#: 421101
Protease Inhibitor Mini Tablets	Thermo Fisher	Cat#: 88665
Cal-Ex II Fixative/Decalcifier	Fisher Chemical	Cat#: CS511-1D
QuikChange II XL Site-Directed Mutagenesis Kit	Agilent	Cat#: 200521
Clopidogrel	Selleck Chemicals	Cat#: S1415
DAPI (4',6-Diamidino-2-Phenylindole, Dilactate)	Biolegend	Cat#: 422801
Critical Commercial Assays		
Urea Nitrogen (BUN) Liqui-UV Test	Stanbio Laboratory	Cat#: 2020-430
Sialyltransferase Activity Kit	R & D systems	Cat#: EA002

(*Continued on next page*)

Continued

REAGENT or RESOURCE	SOURCE	IDENTIFIER
Glycosyltransferase Activity Kit	R & D systems	Cat#: EA001
Experimental Models: Cell Lines		
Expi293F Cells	Thermo Fisher	RRID: CVCL_D615 Cat#: A14527
Experimental Models: Organisms/Strains		
Mouse: C57BL/6J	The Jackson Laboratory	RRID: IMSR_JAX:000664
Mouse: B6.129S2(C)-*Stat6*^{tm1Gru}/J	The Jackson Laboratory	RRID: IMSR_JAX:005977
Mouse: B6.129S4-*Fcgr2b*^{tm1TtK} N12	Taconic	RRID: IMSR_TAC:2621
Mouse: B6.129P2-Cd209b^{tm1Anjm} (SIGN-R1$^{-/-}$)	Lanoue et al., 2004	RRID: MGI:3525070
Mouse: B6.hDC-SIGN/SIGN-R1$^{-/-}$	Anthony et al., 2011	N/A
Mouse: NOD/ShiLtJ	The Jackson Laboratory	RRID: IMSR_JAX:001976
Mouse: KRN TCR Tg	Kouskoff et al., 1996	N/A
Oligonucleotides		
Primers used in this study, see Table S1	This study	N/A
Recombinant DNA		
Human IgG-Fc fused ST6GAL1	This study	N/A
Human IgG-Fc fused B4GALT1	This study	N/A
Software and Algorithms		
GraphPad Prism 7	GraphPad Software	https://www.graphpad.com/scientific-software/prism/
OpenLAB software	Agilent	N/A
imageJ	N/A	https://imagej.nih.gov/ij/index.html
ImmunoRatio	N/A	Tuominen et al., 2010
Other		
Agilent AdvanceBio Glycan Mapping column (120Å, 2.1 × 150 mm, 2.7 μm)	Agilent	Cat#: 683775-913

CONTACT FOR REAGENT AND RESOURCE SHARING

Further information and requests for resources and reagents should be directed to and will be fulfilled by the Lead Contact, Robert M. Anthony (robert.anthony@mgh.harvard.edu).

EXPERIMENTAL MODEL AND SUBJECT DETAILS

Cell culture

Expi293 Cell (Thermo Fisher) was used to produce all recombinant proteins. Cells were grown on orbital shaker (125rpm) in Expi293 Expression Medium (Thermo Fisher) at 37°C in 5% CO_2.

In vivo animal studies

Group housed 7 – 8 weeks old female WT C57BL/6, STAT6$^{-/-}$ and NOD mice were purchased from the Jackson Laboratory and maintained in the animal facility at Massachusetts General Hospital (MGH) under specific pathogen free conditions, and given food and water *ad libitum* according to the National Institutes of Health (NIH) guidelines. SIGN-R1$^{-/-}$(CD209b) and hDC-SIGN^{+}/SIGN-R1$^{-/-}$ mice on a C57BL/6 background were gifts from J. Ravetch (The Rockefeller University, New York, NY) KRN TCR transgenic mice on a C57BL/6 background (K/B) were gifts from D. Mathis and C. Benoist (Harvard Medical School, Boston, MA) and were bred to NOD mice to generate K/BxN mice (Korganow et al., 1999). K/BxN mice with visible disease were bled, and serum was separated from the blood by serum collection tubes (BD), as described previously (Kaneko et al., 2006b).

In vivo Platelet Inhibition Treatment

Platelet inhibition was performed by daily intraperitoneal injections of 10 mg/kg clopidogrel (Selleckchem) as previously described (Pucci et al., 2016), 30 mg/kg ozagrel HCl (Selleckchem) as described (Ishitsuka et al., 2009) and 30 mg/kg sulfinpyrazone

(Selleckchem) (Raeder et al., 1982). Treatment was initiated 2 days before K/BxN sera in the inflammatory arthritis model. In the nephrotoxic nephritis model, treatment was initiated 2 days after pre-immunization with sheep IgG. Treatment was continued for duration of the experiment.

METHOD DETAILS

Construction of glycosyltranserase fusions

Human IgG Fc, preceded by IL2 secretion signal sequence, and soluble domains of ST6GAL1 (Beta-galactoside alpha-2,6 sialyltransferase 1) or B4GALT1 (Beta-1,4-galactosyltransferase 1) were joined by overlapping PCR, such that human IgG Fc is fused to 5′ end of the enzymes. List of primers used in this study is summarized in Key Resources Table. The Fc-enzyme fusion genes were then TOPO cloned into a mammalian expression vector, pcDNA3.4, according to the manufacturer's protocol (Life Technologies). Recombinant Fc-enzymes were generated by transient transfection of the plasmids to Expi293 cells using Expi293 Expression System Kit (Life Technologies) according to the manufacturer's protocol. B4ST6^{Fc} enzyme was produced by co-transfecting pcDNA3.4/ST6^{Fc} and pcDNA3.4/B4^{Fc} at a 1:1 ratio. The enzymes were purified from the culture supernatant using Protein G agarose beads (Thermo Scientific) and dialyzed in PBS for *in vivo* injections.

In vitro glycosylation

Enzymatic activity of fusion enzymes was examined *in vitro* as previously described (Anthony et al., 2008a). Briefly, glycan-acceptor protein (fetuin, human or mouse IgG Fc) was treated with Sialidase A (ProZyme) and β1,4-galactosidase-S (New England Biolabs) overnight at 37°C to remove sialic acid and galactose. To assess the galactosyltransferase activity of B4^{Fc} or B4ST6^{Fc}, asialylated, agalactosylated glycan-acceptor protein was incubated with 5mM UDP-galactose (Calbiochem) in 2 × galactosylation buffer (50mM MOPS, 20mM $MnCl_2$, pH7.2) overnight at 37°C. To assess the sialyltransferase activity of ST6^{Fc} or B4ST6^{Fc}, asialylated glycoprotein was incubated with 5mM CMP-sialic acid (Nacalai tesque) in the sialylation buffer (150mM NaCl, 20mM HEPES, pH7.4) overnight at 37°C.

Western and Lectin Blots

Western and lectin blots were performed as described previously (Anthony et al., 2008a). Briefly, equal amounts of protein were resolved on 4 – 12% Bis-Tris SDS-PAGE gel (Life Technologies) and then transferred to polyvinylidene difluoride membranes. After blocking the membranes with 5% dry milk in PBST (0.05% Tween 20) for western blot, proteins were detected using either anti-human IgG-HRP (20ng/ml, Promega); anti-human B4GALT1 (100ng/ml, Sigma-Aldrich) followed by anti-rabbit IgG-HRP (50ng/ml, Promega); or anti-human ST6GAL1 sera (1:100, generous gift from Dr. J. Paulson) followed by anti-rabbit IgG-HRP. For lectin blots, the membranes were blocked in Protein Free Blocking Buffer (Thermo Fisher Scientific), and probed with either biotinylated Sambucus Nigra Lectin (SNA; 5 μg/ml, Vector Laboratories) or with biotinylated Erythrina Cristagalli Lectin (ECL; 5 μg/ml, Vector Laboratories) to detect terminal sialic acid or galactose, respectively.

HPLC Glycan Analysis

Total or Fc specific N-linked glycan was released from glycoproteins using PNGaseF or EndoS (New England Biolabs), respectively, according to manufacturer's instruction. Deglycosylation reactions were carried out at 37°C overnight to ensure effective release of glycans. Glycans were purified from the reaction using GlykoClean G Cartridges (Prozyme), dried, and fluorescently labeled with 2-AB (2-aminobenzamide) (Sigma-Aldrich). Labeled glycans were cleaned with GlykoClean S-plus Cartridges (Prozyme), dried, and subjected to HPLC analysis. Glycan samples were dissolved in 100mM ammonium formate (pH4.5) and separated using Agilent 1260 Infinity Quaternary LC system, outfitted with AdvanceBio Glycan Mapping column 2.1 × 150mm, 2.7 μm and a fluorescent detector. Resulting peaks were analyzed in OpenLAB software (Agilent) and assigned glycoforms by comparing peaks to human IgG N-linked glycan standards (Agilent).

K/BxN serum transfer

Inflammatory arthritis was induced by intravenous injection of K/BxN sera (200 μL of pooled K/BxN serum per mouse). For therapeutic intervention experiments, IVIG (1g/kg), B4^{Fc} (1.25mg/kg or 2.5mg/kg), ST6^{Fc} (1.25mg/kg or 2.5mg/kg), B4ST6^{Fc} (2.5mg/kg), or saline was injected one hour prior to K/BxN serum (day 0), or on day 3 after K/BxN serum. Arthritis was scored by clinical examination, and the index of all four paws was added (0 = unaffected, 1 = swelling of one joint, 2 = swelling of more than one joint, 3 = severe swelling of the entire paw) as described (Kaneko et al., 2006b).

Nephrotoxic nephritis

Mice were pre-immunized with 200 μg of sheep IgG (BioRad) in CFA via intraperitoneal route, followed by intravenous injection of sheep NTS (Probetex) (2 μL of serum per gram of mouse) 4 days later. IVIG (1g/kg), B4ST6^{Fc} (50 μg) or PBS was injected 1 hour before sheep NTS injection. Urea nitrogen (BUN) in sera was measured by the enzyme coupled equilibrium method using a modified urease kit (Stanbio Laboratory). Moribund animals were euthanized by CO_2 asphyxiation. All animal experiments were conducted in compliance with the Institutional Animal Care and Use Committee of MGH.

ELISA

96-well ELISA plates coated with 5 μg/mL of sheep IgG were incubated with 1:500 diluted sera after blocking with 5% bovine serum albumin. After washing with PBS containing 0.05% Tween 20, the plates were incubated with HRP conjugated anti-mouse IgG-Fc (Bethyl Laboratories). The amount of IgG bound was assessed by 3,3′, 5,5′-tetramethylbensidine (TMB; Biolegend) and the absorbance measured at 450 nm after 2M sulfuric acid addition.

Kidney and joint IgG purification

Mice were bled on days 4, and 7 after anti-GBM antiserum injection. The serum was separated from the blood by serum gel tubes (BD) and incubated with Protein G high-capacity agarose beads (Thermo Fisher Scientific) for IgG purification. Paws were removed just above ankle joints and kidneys were dissected, suspended in 1mL PBS supplemented with protease inhibitor and 2mM EDTA and cut into small pieces before mechanical homogenization stainless steel beads and TissueLyser II (QIAGEN) for two minutes at 3Hz/s. Homogenate was then diluted 5-fold by volume in PBS with Protein Inhibitor (Thermo) and 2mM EDTA, filtered through 70 μm mesh, and centrifuged at 1000 × g for 5 min. Protein G high-capacity agarose beads was applied to the supernatant to purify IgG.

Histology

Ankle joints were dissected and incubated in the fixative and decalcifier solution Cal-Ex II for 48hrs-72hrs (Fisher Chemical), and embedded in paraffin. 4 μm sections were stained with hematoxylin/eosin for histological analysis. Kidneys were dissected, fixed in 10% buffered formalin and embedded in paraffin. 4 μm paraffin sections were stained with Trichrome mason, periodic acid-schiff (PAS), and hematoxylin/eosin for analysis by light microscope. For immunofluorescent tissue staining, 4 μm OCT (Tissue –Tek) frozen kidneys sections were fixed in acetone and stained, where indicated, with DAPI (Biolegend) or rabbit anti-mouse IgG-Fc specific-DyLight405 (Jackson ImmunoResearch) in combination with rat anti-mouse CD41-APC (Biolegend), rat anti-mouse CD62P-PE (Biolegend), and goat anti-mouse Nephrin (R&D Systems) followed by donkey anti-goat IgG-AF488 (Jackson ImmunoResearch), F4/80-PE (Biolegend), SIGNR1-Alexa647 (eBioscience), DC-SIGN-Alexa647 (Biolegend) according to manufacturer's instructions. Immunohistochemistry to identify platelets via rat anti-CD41-Biotin (Biolegend) staining was also performed on paraffin embedded sections of kidneys and paws. Slides were examined using a fluorescence microscope (Carl Zeiss). 200x joint images, and 400x kidney images were captured, and assembled, including insets, using ScientiFig v.3.1 (Aigouy and Mirouse, 2013).

Glomerulosclerosis and platelet infiltration

Glomerulosclerosis score was evaluated as described (Schwarzenberger et al., 2015) with slight modifications. Briefly, at least 50 randomly selected glomeruli on PAS-stained tissue sections were evaluated under 400X magnification and scored using a semiquantitative scoring system from 0 to 4, where 0 = normal glomeruli without structural damage, 1 = glomerular matrix expansion and edema formation of less than 25% of the glomerulus, 2 = increased intraglomerular cell count and swelling up to 50%, 3 = obliteration or collapse of glomerulus up to 75% of the glomerular cross-section, and 4 = complete structural obliteration and thrombosis. Glomerular Platelet infiltration was determined as the percentage of CD41-DAB to hematoxylin staining as determined by ImmuneRatio software (Tuominen et al., 2010).

Platelet preparation

Platelet isolation, activation and inhibition were adapted from past studies (Boilard et al., 2010; Lee et al., 2014). Eight healthy individuals aged of 20 to 50 of both sex gave informed consent, and whole blood was collected in sodium citrate buffered blood collection tubes (BD) pre-warmed to 37°C and centrifuged for 10 min at 200 × g. The platelet rich plasma (PRP) in supernatant was collected and further centrifuged for 5 min at 900 × g to collect platelets. After removing the platelet poor plasma in supernatant the pelleted platelets were gently washed and resuspended with pre-warmed platelet resuspention buffer: 140mM NaCl, 3mM KCl, 0.5mM $MgCl_2$, 5mM $NaHCO_3$, 10mM D-glucose, 10mM HEPES, pH 7.4. Platelet activation was achieved using 0.2U of thrombin (Roche) for 5min at 37°C. Platelet activation was inhibited using 0.25mg of Clopidogrel for 15 min at room temperature, followed by 0.2U thrombin treatment for 5 min at 37°C. Platelets were pelleted by centrifugation at 1000 × g for 5min, and the supernatant was quantified for UDP-Galactose and CMP-SA. Samples were processed at room temperature or 37°C, wide-bore pipets tips were used, and all centrifuge spins were performed with no brakes applied to avoid spontaneous platelet activation.

Quantification of UDP-Gal and CMP-SA

Quantitation of the glycan donor was performed on human platelet supernatant using sialyltransferase and glycosyltransferase activity kit as indicated by the manufacturer (R & D systems), with one exception. Standard curves were generated using a range of UDP-Gal and CMP-SA in order to more accurately report the concentration.

Serum Half-life Experiments

50 μg of human IgG-Fc, $B4^{Fc}$, $ST6^{Fc}$ or $B4ST6^{Fc}$ was intravenously administered to C57BL/6 female mice. The mice they were bled 1, 2, 4, 6, 8, 10 days after the injection. Injected protein in mice sera was detected by ELISA. Briefly, 96-well plates were coated

with 5 μg/ml of anti-human IgG Fc (Bethyl Laboratories), blocked with 2% BSA in PBS, and probed with anti-human IgG-HRP (20ng/ml, Promega). 3,3,5,5-tetramethylbenzidine (TMB; Thermo Fisher Scientific) was used for the detection, and 2M sulfuric acid was used to stop the reaction.

Blood testing

50 μg of $B4ST6^{Fc}$ was intravenously injected to mice. After 1 week or 2 months of the administration of the enzyme the mice were bled, and whole blood and sera were sent to MGH Histopathology Research Core for HemaTrue complete blood count (CBC) and comprehensive metabolic panel tests.

QUANTIFICATION AND STATISTICAL ANALYSIS

General. Data were analyzed in GraphPad Prism: *$p < 0.05$, **$p < 0.01$, ***$p < 0.005$, ****$p < 0.001$ as determined by two-way ANOVA followed by Tukey's posthoc.

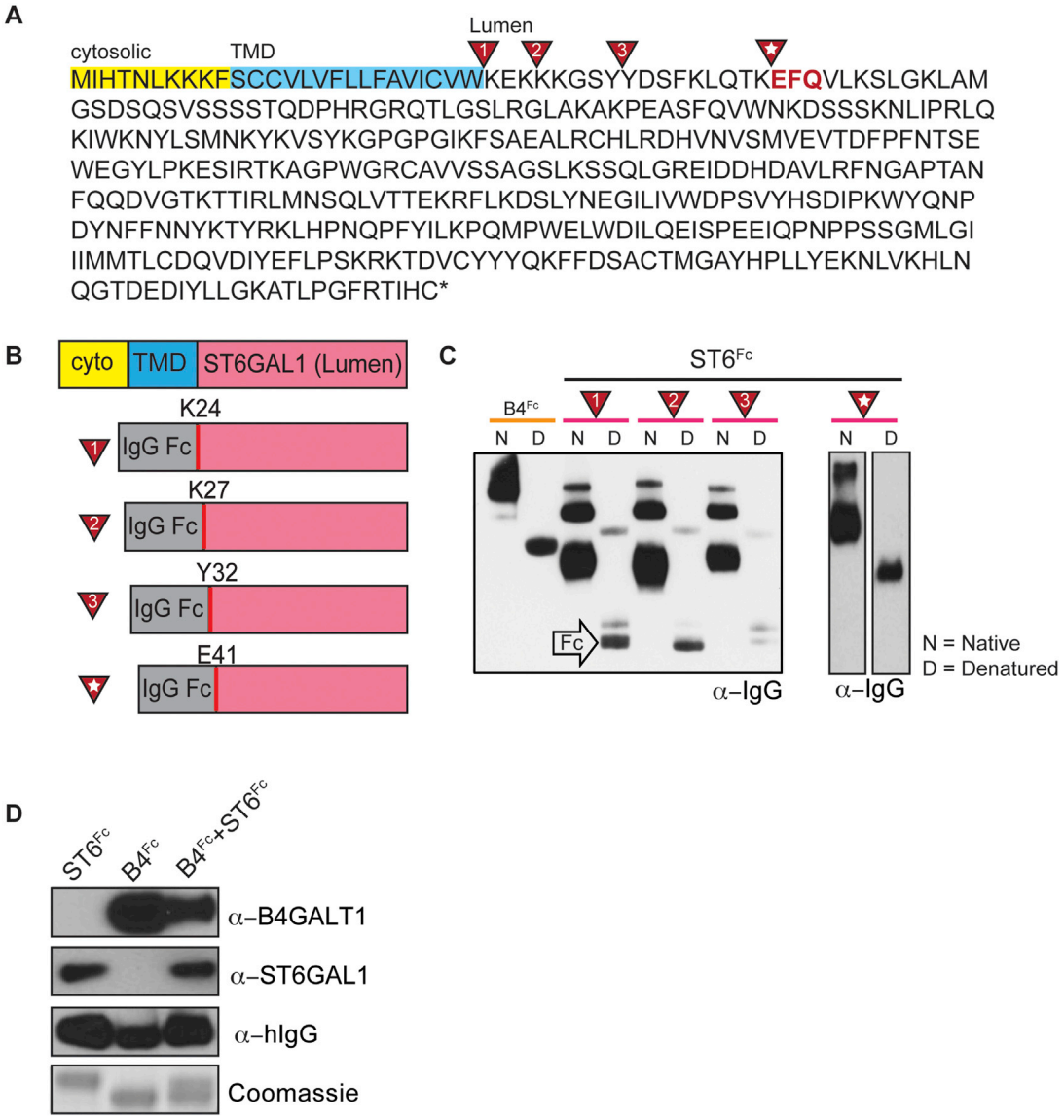

Figure S1. Engineering and Characterization of Soluble Galactosyl- and Sialyltransferase Proteins, Related to Figure 1

(A) Protein sequence of human ST6GAL1. Yellow and light blue shaded sequences represent cytosolic and transmembrane domain (TMD), respectively. Numbered red triangles indicate the start site of the sialyltransferase which was fused to IgG Fc. The triangle with a star indicates the start site of the soluble ST6GAL1 that was used in all experiments in this manuscript.

(B) Schematic representations of each ST6GAL1 are shown.

(C) Immunoblots of Fc-enzyme proteins for reactivity to IgG (N, native protein; D, denatured protein). ST6Fcs were cleaved to Fc and ST6GAL1 upon denaturation when fused upstream of EFQ41-43. The lanes are separated because of unrelated samples loaded between native and denatured ST6Fc on the same gel.

(D) Immunoblots of $ST6^{Fc}$, $B4^{Fc}$, and $B4ST6^{Fc}$ for reactivity to B4GALT1, ST6GAL1, or IgG.

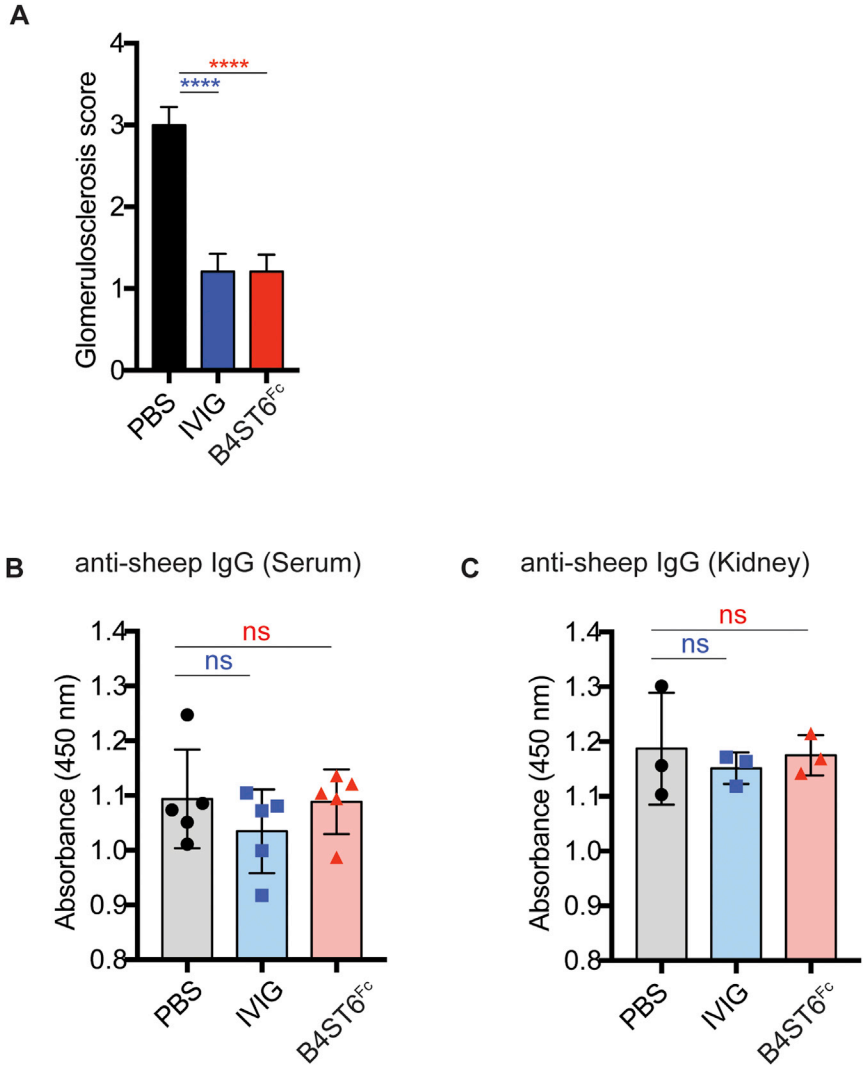

Figure S2. Glomeruli Inflammation and the Anti-sheep Response after NTN Induction and B4ST6^{Fc}, Related to Figure 2

(A) Glomerulosclerosis score was plotted 7 days after NTN-induction with PBS (black), high dose IVIG (blue), and B4ST6^{Fc} (red) treatment.

(B and C) Day 7 anti-sheep IgG titers from the serum (B) or kidney (C) from NTN-induced mice were treated with PBS (black circles), high dose IVIG (blue squares), or B4ST6^{Fc} (2.5mg/kg) (red triangles) were determined by ELISA.

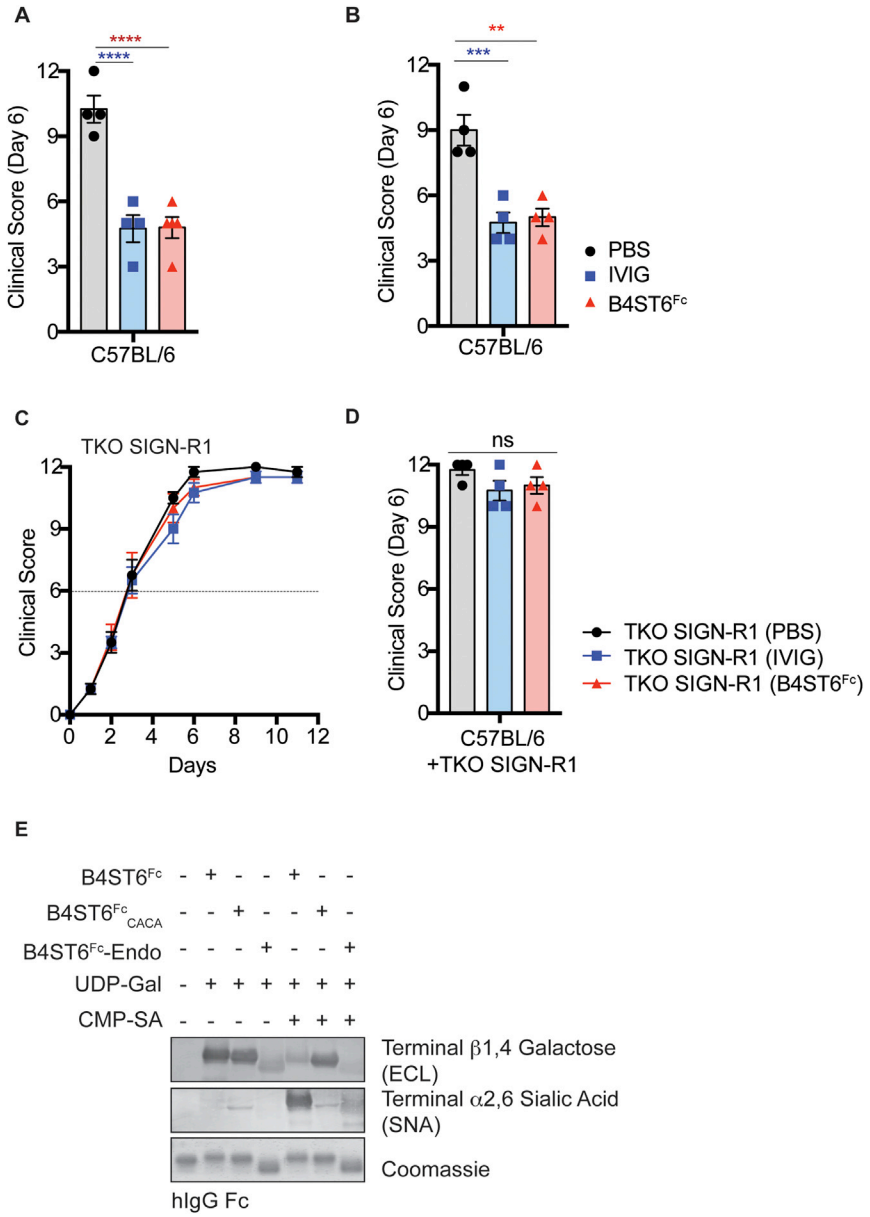

Figure S3. IVIG and B4ST6^{Fc} Anti-inflammatory Activity in Wild-Type Controls and SIGN-R1-TKO Animals and *In Vitro* Enzymatic Activity of ST6$^{Fc}_{CACA}$ and EndoS-Treated ST6^{Fc}, Related to Figures 3 and 4

(A and B) Day 6 clinical scores of control C57BL/6 mice after K/BxN injection for Figures 3A and 3C, respectively. These are from control groups for FcγRIIB$^{-/-}$ (A) and STAT6$^{-/-}$ (B) treatments shown in Figures 3A–3D. Results are representative of at least two independent repeats.

(C) C57BL/6 mice were given SIGN-R1 blocking antibody (TKO SIGN-R1), K/BxN sera, and PBS (black circles), IVIG (blue squares), or B4ST6^{Fc} (red triangles). Paw swelling was monitored over several days.

(D) Day 6 clinical scores of individual mice from (C) are shown. *$p < 0.05$, **$p < 0.01$, ***$p < 0.005$, ****$p < 0.001$, ns (not significant), determined by two-way ANOVA followed by Tukey's posthoc.

(E) Linkage-specific lectin blots assaying for terminal β1,4 galactose (ECL) or α2,6 sialic acid (SNA) on human IgG Fcs following incubation with B4ST6^{Fc}, B4ST6$^{Fc}_{CACA}$, or B4ST6^{Fc}-Endo. Galactosylation was assayed by incubation with UDP-Gal on (G0) IgG Fc. Sialyltransferase activity was evaluated by incubation with CMP-SA on (G2) IgG Fc.

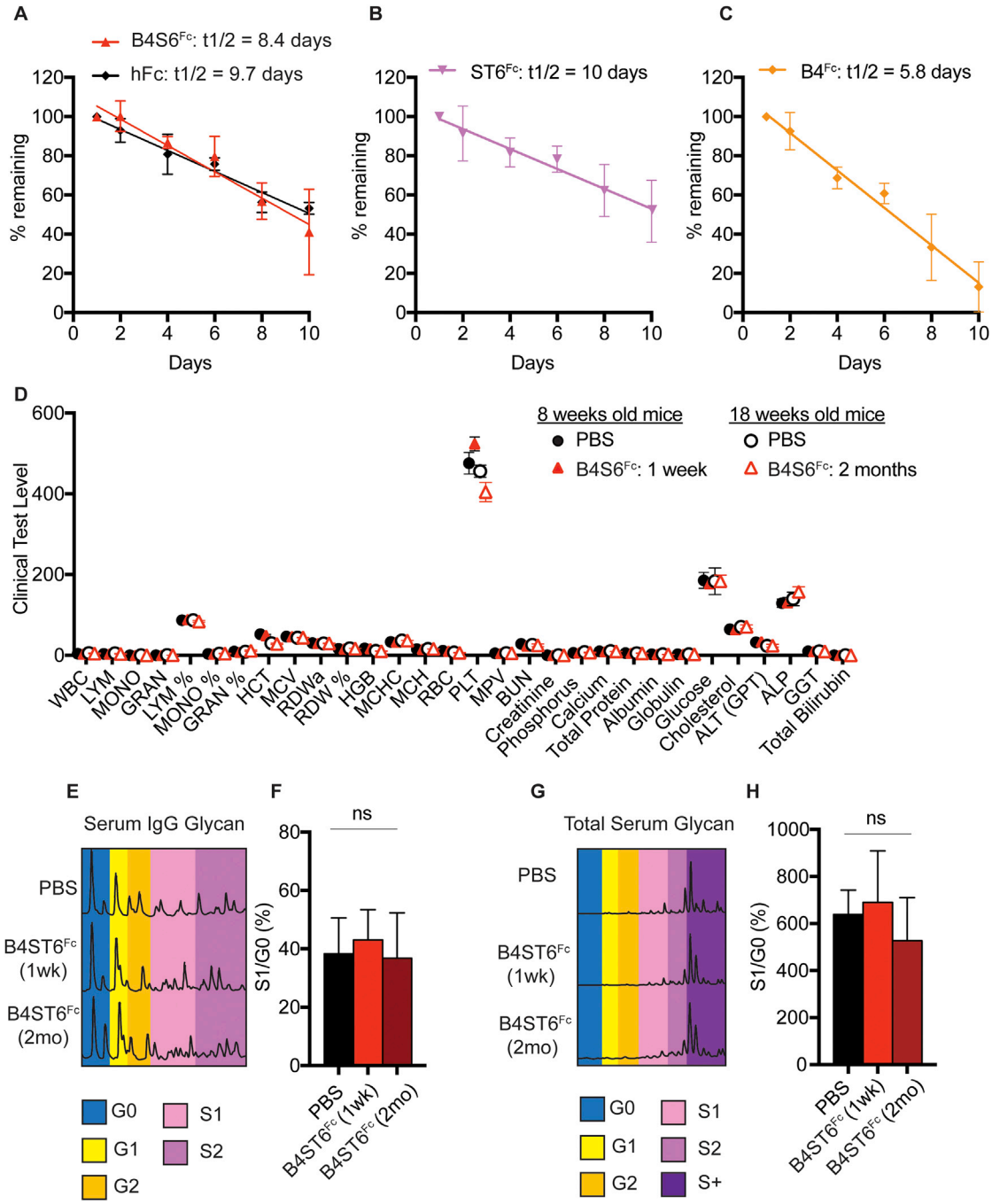

Figure S4. *In Vivo* Sialylation during Homeostasis, Related to Figures 3 and 4

(A–C) Serum concentrations of human IgG-Fc and B4ST6^{Fc} (A), ST6^{Fc} (B), and B4^{Fc} (C) at defined intervals after administration are plotted with half-lives inset.

(D) Blood test values following administration of PBS (black circles) or B4ST6^{Fc} one week earlier (red triangles) for 8 weeks old mice, and PBS (open black circle) or B4ST6^{Fc} two months earlier (open red triangles) for 18 weeks old mice. WBC, white blood cell; LYM, lymphocytes; MONO, monocytes; GRAN, granulocytes; HCT, hematocrit; MCV, mean corpuscular volume; RDW, red blood cell distribution width; HGB, hemoglobin; MCHC, mean corpuscular hemoglobin concentration; MCH, mean corpuscular hemoglobin; RBC, red blood cell (erythrocyte) count; PLT, platelet; MPV, mean platelet volume; BUN, blood urea nitrogen; ALT (GPT), Alanine Amino Transferase; ALP, alkaline phosphatase; GGT, Gamma-Glutamyl Transferase.

(E) Glycan HPLC traces of serum IgG recovered after 1 week or 2 months of the administration of B4ST6^{Fc}. Shading corresponds to retention time of terminal sugar (blue, G0; yellow, G1; orange, two G2; pink, one S1; purple, S2).

(F) Ratios of mono-sialylated and agalactosylated glycans (S1/G0) from IgG described in (E) are shown.

(G) HPLC traces of total serum glycan after 1 week or 2 months of the administration of B4ST6^{Fc}.

(H) Ratios of mono-sialylated and agalactosylated glycans (S1/G0) from IgG described in (G) are shown.

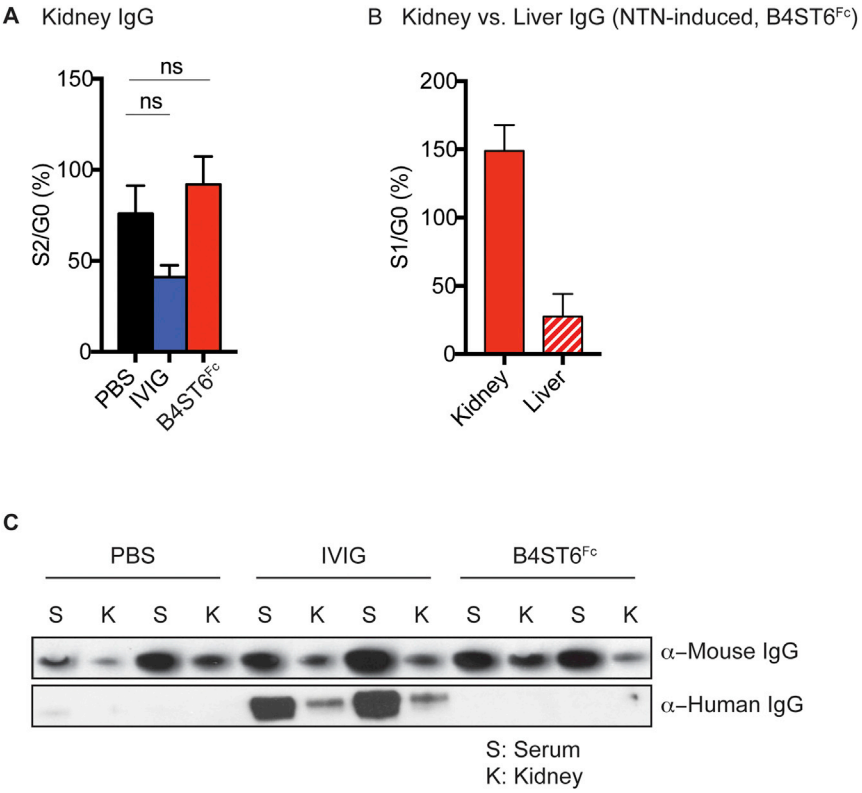

Figure S5. Site-Specific *In Vivo* Sialylation during Inflammation, Related to Figure 6

(A) Ratios of di-sialylated and agalactosylated glycans (S2/G0) IgG recovered from kidney of NTN-induced mice.

(B) Ratios of mono-sialylated and agalactosylated glycans (S1/G0) from IgG recovered from kidney or liver 7 days after NTN-induction and B4ST6^{Fc} administration.

(C) Total IgG purified from serum and kidney of NTN-treated mice received PBS, IVIG, or B4ST6^{Fc} was probed by immunoblotting for mouse and human IgG.

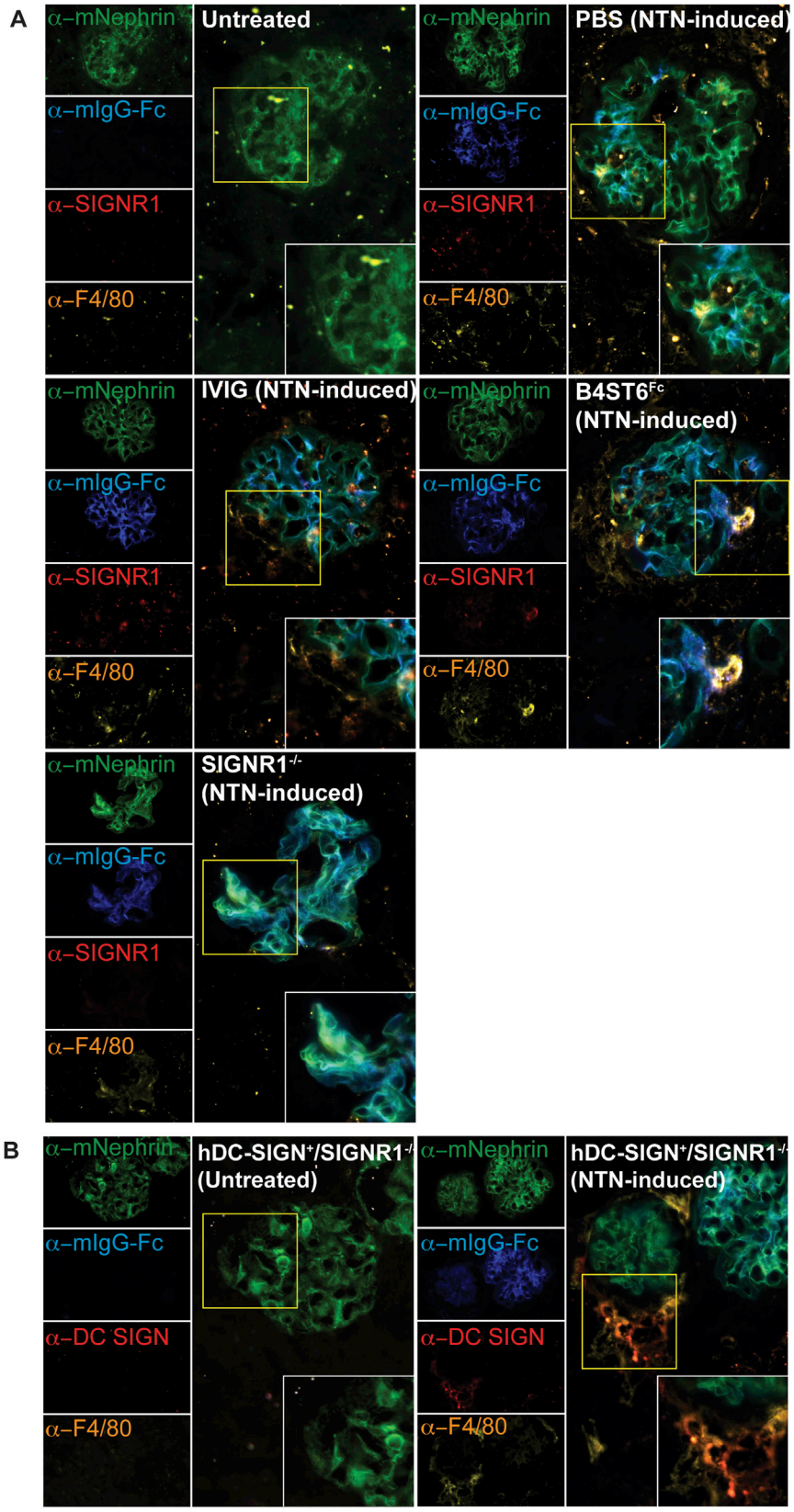

(legend on next page)

Figure S6. Type II FcγR^{+} Macrophages in Kidneys following NTN Induction, Related to Figure 6

(A) C57BL/6 or SIGN-R1$^{-/-}$ mice were NTN-induced and given PBS, IVIG or B4ST6^{Fc}. Kidneys of these mice were examined for glomeruli (mNephrin, green), mIgG-Fc (blue), SIGN-R1 (red), macrophage (yellow). Representative individual and overlayed images are shown.

(B) DC-SIGN^{+}/SIGN-R1$^{-/-}$ mice were left untreated or NTN-induced. 7 days after the disease induction, kidneys were examined for glomeruli (mNephrin, green), mIgG-Fc (blue), DC-SIGN (red), macrophage (yellow). Representative individual and overlayed images are shown.

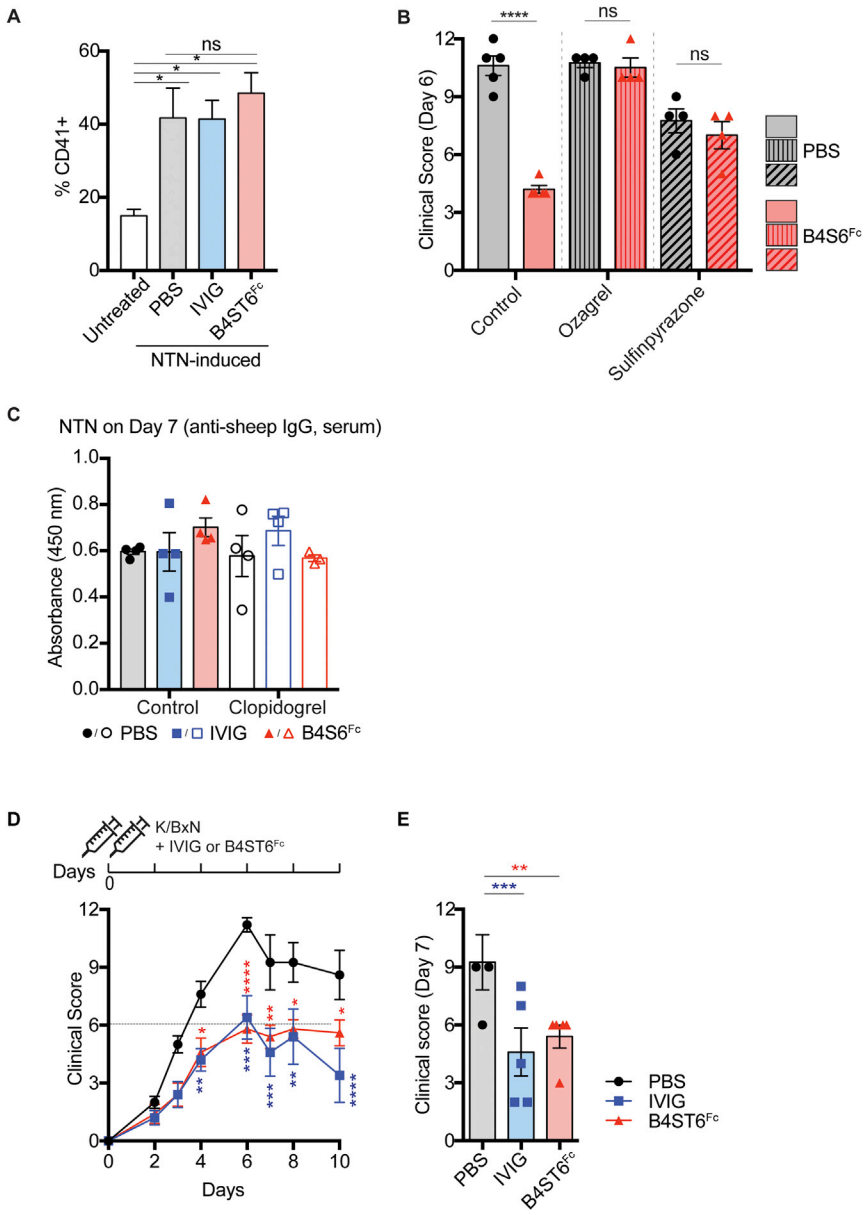

Figure S7. Platelet Inhibition Prevents B4ST6^{Fc} Anti-inflammatory Activity and Therapeutic Potential of the *In Vivo* Sialylation, Related to Figures 6 and 7

(A) Kidneys of untreated and day 7 NTN-induced mice following treatment with PBS, IVIG and B4ST6^{Fc} were examined for presence of platelet CD41 (representative image shown in Figure 6A) and platelet accumulation was quantified by plotting the percentage of CD41-DAB to hematoxylin as determined by ImmuneRatio application (Tuominen et al., 2010).

(B) K/BxN sera were given to control (no drug), ozagrel treated, or sulfinpyrazone treated mice followed by PBS or B4ST6^{Fc} administration. Paw swelling was monitored over several days and Day 6 clinical score is plotted.

(C) Day 7 anti-sheep IgG titers of NTN-induced mice were treated with PBS (black circles), high dose IVIG (blue squares), or B4ST6^{Fc} (2.5mg/kg) (red triangles) some of which also received clopidogrel. *$p < 0.05$, **$p < 0.01$, ***$p < 0.005$, ****$p < 0.001$, ns (not significant), determined by two-way ANOVA followed by Tukey's posthoc.

(D) K/BxN treated mice were given PBS (black circles), IVIG (blue squares), or B4ST6^{Fc} (red triangles) on day 0 and paw swelling monitored over several days.

(E) Day 7 clinical scores of individual mice from (D) are shown. These are control groups for data shown in Figures 7E and 7F.